

Modulation of glymphatic system by visual circuit activation alleviates memory impairment and apathy in a mouse model of Alzheimer's disease

Received: 13 April 2024

Accepted: 20 December 2024

Published online: 02 January 2025

 Check for updates

Wen Wu^{1,16}  , Yubai Zhao^{1,2,16}, Xin Cheng^{3,4,5,16}, Xiaoru Xie^{5,6,7,8}, Yixiu Zeng^{3,4,5}, Quan Tao¹, Yishuai Yang⁵, Chuan Xiao^{5,6,7,8}, Zhan Zhang^{5,6,7,8}, Jiahui Pang¹, Jian Jin¹, Hongbo He⁹, Yangyang Lin^{10,11,12}, Boxing Li^{5,13,14}, Junxian Ma¹⁵  , Xiaojing Ye^{3,4,5}   & Wei-Jye Lin^{5,6,7,8}  

Alzheimer's disease is characterized by progressive amyloid deposition and cognitive decline, yet the pathological mechanisms and treatments remain elusive. Here we report the therapeutic potential of low-intensity 40 hertz blue light exposure in a 5xFAD mouse model of Alzheimer's disease. Our findings reveal that light treatment prevents memory decline in 4-month-old 5xFAD mice and motivation loss in 14-month-old 5xFAD mice, accompanied by restoration of glial water channel aquaporin-4 polarity, improved brain drainage efficiency, and a reduction in hippocampal lipid accumulation. We further demonstrate the beneficial effects of 40 hertz blue light are mediated through the activation of the vLGN/IGL-Re visual circuit. Notably, concomitant use of anti-A β antibody with 40 hertz blue light demonstrates improved soluble A β clearance and cognitive performance in 5xFAD mice. These findings offer functional evidence on the therapeutic effects of 40 hertz blue light in A β -related pathologies and suggest its potential as a supplementary strategy to augment the efficacy of antibody-based therapy.

Alzheimer's disease (AD) is the leading cause of dementia in the elderly and poses substantial medical and social burdens worldwide^{1,2}. Recent advancement in anti-A β immunotherapy have shown positive clinical outcomes for early-stage AD, preserving cognitive function and reducing amyloid accumulation in the brains of patients, leading to its approval for clinical use³. However, despite these advancements, anti-A β immunotherapy carries the risk of amyloid-related imaging abnormalities (ARIA) in a dose-dependent manner, and can result in severe adverse events⁴. Therefore, the identification of alternative treatment options, either alone or in combination with low-dose anti-A β immunotherapy, holds great value for AD intervention.

Light treatment has been utilized to improve cognitive function in patients with early-to-middle-stage AD for decades, though its effect on middle-to-late-stage AD renders further evaluation⁵⁻⁸. Studies reported that the non-visual effect of light, such as regulation of mood and cognition, is mediated by the intrinsically photosensitive retinal ganglion cells (ipRGCs), which exhibit the highest sensitivity to blue light^{9,10}. A study found that blue-enriched light had a better effect on alertness and mood compared to white light¹¹. Moreover, morning blue-enriched illumination for 2 weeks has been found to improve sleep and cognitive function in patients with mild to moderate AD¹². Previous studies have also suggested that 40 Hz light flickers, as opposed to constant light or other frequencies, are particularly

A full list of affiliations appears at the end of the paper.  e-mail: wuwen66@163.com; 931616518@qq.com; yexiao8@mail.sysu.edu.cn; linwj26@mail.sysu.edu.cn

effective for improving cognitive functions in AD patients and mouse models^{13,14}. However, the underlying mechanisms are still under debate. While early studies propose that 40 Hz light treatment entrains gamma oscillation, reduces A β deposits and mitigates microglia activation, these findings have been disputed by subsequent research^{14–16}. Further investigation is necessary to elucidate the mechanisms underlying the beneficial effects of 40 Hz light therapy in AD.

The recently discovered glymphatic drainage system has been proposed to play an important role in A β clearance¹⁷. The glymphatic system is a brain-wide perivascular pathway that facilitates the clearance of interstitial fluid (ISF) and solutes, such as soluble A β , into the cerebrospinal fluid (CSF) and then to the periphery through meningeal and cervical lymphatic vessels^{18,19}. This clearance system is regulated by the water channel aquaporin-4 (AQP4) on the perivascular astrocytic endfeet^{19,20}. The glymphatic drainage has been found to be suppressed in the early stages of AD, contributing to A β plaque accumulation and memory deficits in mouse models of AD pathology^{21,22}. In AD patients, there is a reduction in the efflux of CSF containing soluble A β ²³. The disruption of perivascular AQP4 has been linked to increased A β burden and cognitive impairment in AD²⁴. Despite this knowledge, treatments to enhance glymphatic drainage remain uncertain. Recent studies have shown that visual light can accelerate glymphatic clearance in the visual cortex (VC) of mice and increase CSF flow in the human brain^{25,26}. This has sparked our interest in exploring whether 40 Hz blue light treatment delays the progression of AD via enhancing the glymphatic drainage efficacy.

In this study, we explored the impact of 40 Hz blue light treatment on glymphatic drainage, A β -related pathology, and cognitive functions in 4- and 14-month-old 5xFAD mice, a widely used β -amyloidopathy mouse model for AD. Our results revealed that the treatment not only enhanced memory performance but also restored motivational behaviors in 5xFAD mice. These improvements were associated with increased glymphatic drainage mediated through the activation of the VLGN/IGL-Re visual circuit. Additionally, concomitant use of anti-A β antibody with 40 Hz blue light enhanced cognitive function and reduced soluble A β in the hippocampus. These findings highlight a visual circuit that underlies the beneficial effects of 40 Hz blue light therapy as a non-invasive treatment strategy for AD.

Results

40 Hz blue light treatment improves memory functions in 4-month-old 5xFAD mice

To explore the therapeutic effects of relatively low-intensity 40 Hz blue light treatment on early-stage AD-related pathology and cognitive decline, we first used 4-month-old 5xFAD mice. At this age, 5xFAD mice begin to exhibit memory deficits²⁷. The mice were exposed to 0.03 mW/cm² (160–180 lux) 40 Hz blue light for 1 h per day for 14 consecutive days, after which they were assessed for spatial working memory function using the Y-maze test, and long-term recognition memory using the novel object recognition test (Fig. 1a). We found that spatial working memory was impaired in 5xFAD mice with no 40 Hz blue light treatment, compared to their wild-type littermates. The 40 Hz blue light treatment effectively alleviated memory impairment in 5xFAD mice without affecting their total exploration activity (Fig. 1b–c). We further investigated the potential benefits of blue light treatment on long-term novel object recognition memory. The results showed that during training, wild-type mice, 5xFAD mice and 5xFAD mice treated with blue light performed similarly in object investigation. However, 5xFAD mice displayed memory deficit during the 24 h memory test, which was significantly alleviated by 40 Hz blue light treatment (Fig. 1d–e). It is worth noting that inappropriately applied light stimuli may increase anxiety levels in mice²⁸. In our study, the application of 40 Hz blue light did not have a significant effect on

anxiety levels or general locomotion, as measured by the open field test (Supplementary Fig. 1a–b).

Of note, the improvement of memory function in 5xFAD mice by 40 Hz blue light was accompanied by an enhancement of c-FOS expression, an indicator for brain activity, in the retrosplenial cortex, the CA3 subregion of the dorsal hippocampus (CA3) and the nucleus reuniens (Re), which are considered important for memory processing^{29–31} (Fig. 1f–g). Additionally, blue light treatment also increased c-FOS expression in the VC and the superior colliculus (SC), important components of the visual pathway^{32,33} (Fig. 1f–g). Interestingly, in 5xFAD mice, we observed an unexpected increase in c-FOS expression in the lateral habenula (LHb), a brain region involved in processing negative emotion, which was significantly reduced after blue light treatment³⁴ (Fig. 1f–g).

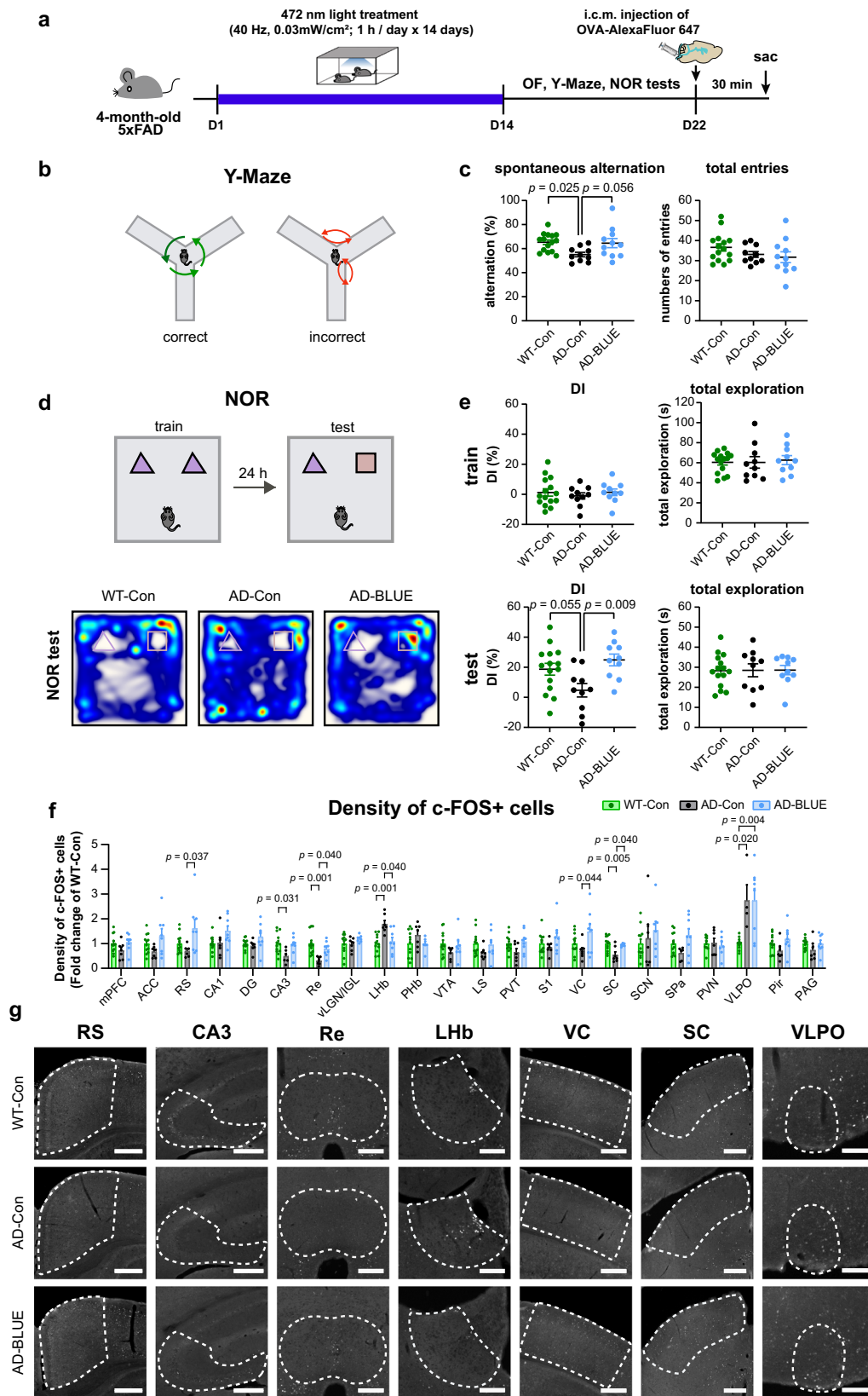
Collectively, our findings demonstrate that low-intensity 40 Hz blue light treatment effectively improves both spatial working memory and long-term recognition memory in 4-month-old 5xFAD mice.

Blue light treatment increases glymphatic drainage in 4-month-old 5xFAD mice

To examine the potential effects of low-intensity 40 Hz blue light treatment on CSF perfusion and clearance in 4-month-old 5xFAD mice, we injected ovalbumin-Alexa Fluor 647 (OVA-AF647) into the cisterna magna after the behavioral tests, and sacrificed the mice 30 min after OVA injection. The distribution and quantity of the OVA-AF647 as a tracer for CSF perfusion in the brain parenchyma were analyzed. We found that blue light treatment significantly enhanced the perfusion of the tracer throughout the entire brain parenchyma in 4-month-old 5xFAD mice (Fig. 2a–b). As CSF can be further drained into the deep cervical lymph nodes (dCLNs)¹⁹, we also analyzed the amount of OVA-AF647 present in the dCLNs. A significant reduction of OVA-AF647 was detected in the dCLNs of 5xFAD mice as compared to their wild-type littermates. However, this reduction was alleviated by blue light treatment (Fig. 2c–d). Furthermore, blue light treatment resulted in a significant reduction of soluble A β 42 in the hippocampus of 5xFAD mice (Fig. 2e). In another cohort of wild-type mice, blue light treatment significantly enhanced the efflux of OVA-AF647 that was injected directly into the hippocampus or striatum (Supplementary Fig. 2).

CSF perfusion and ISF clearance can be enhanced through two different ways: improving the meningeal lymphatic pathway in the dura mater, or improving the glymphatic system in the brain parenchyma^{35,36}. To investigate these possibilities, we first performed immunofluorescence staining of lymphatic vessel endothelial hyaluronan receptor 1 (LYVE1) to label meningeal lymphatics in the dura mater. We observed a small yet significant reduction in the diameter of meningeal lymphatics of 5xFAD mice compared to their wild-type littermates, which, however, was not rescued by blue light treatment, analyzed at either after eight days of behavioral testing or one day following the completion of a 14-day regimen of 40 Hz blue light treatment (Supplementary Fig. 3a–b, c–d, g–h). Additionally, the fluorescent intensity of LYVE1 staining or the area covered by meningeal lymphatics remained unaltered following blue light treatment, suggesting that blue light treatment had limited effect on the meningeal lymphatics (Supplementary Fig. 3e–f, i–j).

The glymphatic system relies on the perivascular localization of the astroglial water channel AQP4 for its clearance function^{37,38}. Using immunofluorescence staining of AQP4, we showed that the perivascular distribution of AQP4 was reduced in the hippocampus and the VC of 5xFAD mice compared to their wild-type littermates, which was significantly alleviated by blue light treatment (Fig. 2f–g). Moreover, blue light treatment also significantly suppressed astrocyte over-activation in the hippocampus and the VC of 5xFAD mice, as indicated by a significant reversal in the elevated ratio of glial fibrillary acidic protein (GFAP) to S100 β level^{39,40} (Supplementary Fig. 4).



Together, these data suggest that blue light treatment effectively alleviates the deficits in CSF perfusion and clearance in the 4-month-old 5x*FAD* mice, which is accompanied by the normalization of perivascular distribution of AQP4 and suppression of astrocyte overactivation, but not alteration of meningeal lymphatic structures.

AQP4 polarity, glymphatic drainage efficiency, and cognitive functions of 5x*FAD* mice are improved by 40 Hz blue light through the activation of vLGN/IGL-Re visual circuit

Neuronal activity of the Re innervated by ventral lateral geniculate nucleus and intergeniculate leaflet (vLGN/IGL) has been reported to mediate the effects of light on hippocampus-dependent memory

Fig. 1 | 40 Hz blue light treatment improves memory functions in 4-month-old 5xFAD mice. **a** The experimental timeline of blue light treatment, behavioral tests, injection of the OVA-Alexa Fluor 647 tracer into the cisterna magna (i.c.m.) and sacrifice (sac). **b** Schematic of the Y-Maze test. **c** The spontaneous alternation and total numbers of arm entries in the Y-maze test ($n = 15, 10, 11$). **d** Upper panel, schematic of the novel object recognition (NOR) test. Lower panel, representative heatmaps of animals' traveling paths during the test session of NOR. **e** Quantification of the discrimination index (DI) and the total time spent on exploring both objects (total exploration) during the training and the test sessions of NOR ($n = 15, 10, 10$). **f** Quantitative analyses of the density of c-FOS positive cells in different brain regions across groups ($n = 12, 7, 8$ of mPFC, ACC, CA1, DG, Re, VTA, LS, PVT, SI, VC, Pir, and PAG; $n = 12, 6, 8$ of RS, CA3, and SPa; $n = 12, 7, 7$ of

vLGN/IGL and SCN; $n = 11, 7, 8$ of LHb; $n = 11, 7, 6$ of PHb; $n = 12, 7, 6$ of SC; $n = 11, 7, 7$ of PVN; $n = 10, 4, 8$ of VLPO). **g** Representative images of c-FOS expression in the retrosplenial cortex (RS; scale bar: 360 μm), cornu ammonis 3 (CA3; scale bars: 360 μm), nucleus reuniens (Re; scale bars: 200 μm), lateral habenula (LHb; scale bars: 150 μm), primary visual cortex (VC; scale bars: 360 μm), the superior colliculus (SC; scale bars: 360 μm) and ventrolateral preoptic area (VLPO; scale bar: 150 μm) brain regions. WT-Con, wild-type littermates that did not receive blue light treatment; AD-Con, 5xFAD mice that did not receive blue light treatment; AD-BLUE, 5xFAD mice that received 40 Hz blue light treatment. All data are presented as the mean \pm SEM and analyzed by one-way ANOVA followed by Tukey's *post hoc* test, except density of c-FOS positive cells in SPa, which are analyzed by Kruskal–Wallis test followed by Dunn's *post hoc* test.

performance⁴¹. In agreement with this, we found a marked enhancement of c-FOS expression in Re after blue light treatment in 4-month-old 5xFAD mice, accompanied with significant improvement in cognitive function, soluble A β 42 clearance and AQP4 polarization in the hippocampus (Fig. 1 and Fig. 2e–g). To further examine whether the 40 Hz blue light could activate Re-projecting vLGN/IGL neurons, we used a monosynaptic retrograde viral strategy to label these neurons (Supplementary Fig. 5a). Acute 40 Hz blue light treatment significantly increased c-FOS expression in the overall vLGN/IGL neurons as well as in the EGFP-labeled Re-projecting vLGN/IGL neurons (Supplementary Fig. 5b–d). These data collectively suggest that low-intensity 40 Hz blue light treatment activated the vLGN/IGL-Re circuit.

We next examined changes in the electrophysiological properties of the Re neurons receiving projections from the vLGN/IGL, which were labeled by a trans-monosynaptic anterograde viral strategy (Supplementary Fig. 5e), following 14 days of blue light treatment. No significant change was observed in the current-evoked action potentials as well as the rheobase current, suggesting a lack of change in their intrinsic excitability (Supplementary Fig. 5f–i). However, there was a significant increase in the spontaneous firing of these Re neurons targeted by vLGN/IGL inputs in mice received 14 days of low-intensity 40 Hz blue light treatment (Supplementary Fig. 5j–k). These findings suggest that blue light treatment altered synaptic activity towards increased activity of these neurons.

To examine the functional roles of the vLGN/IGL-Re pathway on the effects of blue light treatment, we employed an hm4Di-based chemogenetic strategy to suppress the neuronal activity of Re neurons receiving projections from vLGN/IGL in 4-month-old 5xFAD mice (Fig. 3a–b). Notably, we found that chemogenetic suppression of Re neurons innervated by vLGN/IGL resulted in blockage of blue light-induced improvement in spatial working memory in the Y-maze test, long-term object recognition memory, glymphatic drainage to the dCLNs, as well as AQP4 polarization in the CA1 and VC of 5xFAD mice, without affecting general locomotion or anxiety levels (Fig. 3c–i, Supplementary Fig. 1c–d). Conversely, increasing the activity of vLGN/IGL-Re circuit by an hm3Dq-based chemogenetic strategy produced similar improvements in cognitive performance, glymphatic drainage, and AQP4 polarization in 5xFAD mice as blue light treatment (Supplementary Fig. 6).

Previous studies have reported the roles of SC-Re and vLGN/IGL-SC circuits in modulating behavioral responses to light^{41,42}. In this study, we also observed increased c-FOS expression in the SC region after 14-day blue light treatment (Fig. 1f–g). To examine whether the SC-Re projection played a role in blue light-mediated effects in 5xFAD mice, we employed an hm4Di-based chemogenetic approach to selectively suppress the activity of Re neurons targeted by SC projections (Supplementary Fig. 7a–b). The results showed that blockage of SC-Re circuit did not alter blue light-mediated effects on cognitive performance as well as AQP4 polarization in 5xFAD mice (Supplementary Fig. 7c–i).

The improved AQP4 polarity in the hippocampus and VC following blue light treatment, or through direct stimulation of the vLGN/IGL-Re circuit, implies these two brain regions may receive projections from Re neurons. Previous studies have documented direct projections from Re to the hippocampus⁴¹. To explore whether the VC also receives direct projections from the vLGN/IGL-Re circuit, we selectively expressed synaptophysin-fused mRuby in Re neurons targeted by vLGN/IGL inputs to label their axonal terminals⁴³. We observed mRuby-positive axonal terminals in the VC, indicating direct innervation from Re neurons that received vLGN/IGL input (Supplementary Fig. 8a–c). These results suggest that the vLGN/IGL-Re circuit may relay the effects of 40 Hz blue light to regulate downstream brain regions such as the hippocampus and VC. In accordance with this, we also noted improvements in AQP4 polarity and a reduction in astrocyte overactivation within the Re region of 5xFAD mice after 40 Hz blue light treatment (Supplementary Fig. 8d–h).

Together, these data suggest that activation of vLGN/IGL-Re visual circuit mediates the improvement effects of blue light treatment on cognitive functions and glymphatic drainage in the 4-month-old 5xFAD mice.

Blockade of brain drainage pathway or AQP4 function prevents the improvement of memory functions in 5xFAD mice by blue light treatment

As our data suggested that blue light treatment effectively enhanced memory function and glymphatic drainage in 4-month-old 5xFAD mice, we next wondered whether the brain drainage pathway was necessary for the beneficial effects. The ISF and solutes are exchanged with CSF and cleared through the glymphatic system, and subsequently drained through the meningeal and then peripheral cervical lymphatic vessels to the dCLNs¹⁹. Therefore, to investigate the potential impact of blocking the brain drainage pathway on the cognitive improvement induced by 40 Hz blue light treatment in 4-month-old 5xFAD mice, we injected intracisternally Dextran-Fluorescein fluorescence dye for visualization of collecting lymphatic vessels anterior to the bilateral dCLNs. This was followed by surgical ablation of the afferent lymphatic vessels to the dCLNs using an electrotope (Fig. 4a), which successfully inhibited the drainage of intracisternally-injected OVA-AF647 into the dCLNs (Fig. 4b–c). In 5xFAD mice that underwent sham surgery, blue light treatment significantly enhanced spatial working memory in the Y-maze test, as well as long-term object recognition memory (Fig. 4d–f). However, ablation of the lymphatic afferents to dCLNs effectively prevented the improvement of both spatial working memory and long-term object recognition memory by blue light treatment (Fig. 4d–f). Neither blue light treatment nor lymphatic vessel ablation had any significant effect on anxiety-like behaviors and general locomotion in the open field test (Supplementary Fig. 1e–f).

To further confirm the involvement of AQP4 in mediating glymphatic drainage and cognitive improvement effects by blue light treatment, 5xFAD mice was administered with TGNO20 to inhibit AQP4

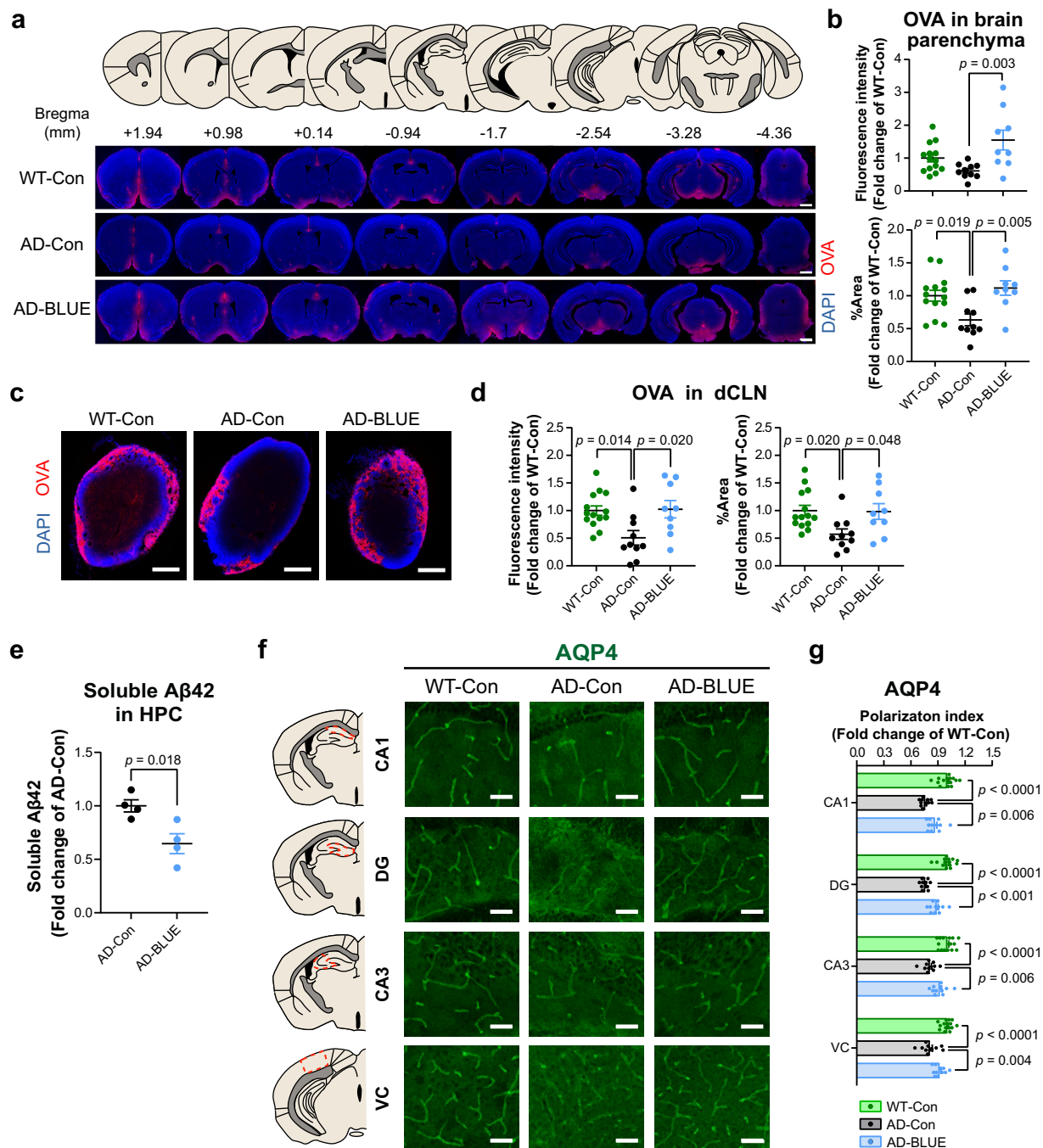


Fig. 2 | 40 Hz blue light treatment increases the glymphatic drainage in 4-month-old 5xFAD mice. **a** Upper panel, the atlas of the brain coronal sections collected. Lower panel, representative images depicting intracisternally-injected OVA tracer (red) distribution. The sections were counterstained with DAPI (blue). Scale bar, 1000 μ m. **b** Quantification of the fluorescence intensity and the percentage of area covered by the OVA tracer in the brain parenchyma ($n = 14, 10, 9$). **c** Representative images depicting OVA tracer (red) and DAPI (blue) staining in the deep cervical lymph nodes (dCLNs). Scale bar, 250 μ m. **d** Quantification of fluorescence intensity and percentage of area covered by the OVA tracer in dCLNs ($n = 14, 10, 9$). **e** Quantification of soluble A β 42 in the hippocampus by ELISA (HPC)

($n = 4, 4$). **f** Representative images of the immunofluorescence staining of AQP4 in the cornu ammonis 1 (CA1), dentate gyrus (DG) and cornu ammonis 3 (CA3) sub-regions of the dorsal hippocampus and the primary visual cortex (VC). Scale bars, 50 μ m. **g** Quantification of the polarization index of AQP4 across different brain regions ($n = 15, 10, 11$). WT-Con, wild-type littermates that did not receive blue light treatment; AD-Con, 5xFAD mice that did not receive blue light treatment; AD-BLUE, 5xFAD mice that received 40 Hz blue light treatment. All data are presented as the mean \pm SEM. Two-group data are analyzed by two-tailed unpaired Student's *t*-test. Three-group data are analyzed by one-way ANOVA followed by Tukey's *post hoc* test.

function during the 14-day regimen of 40 Hz blue light treatment (Fig. 5a). Suppression of AQP4 function effectively abrogated the beneficial effects of 40 Hz blue light treatment on spatial working memory in the Y-maze test, as well as long-term object recognition memory, without affecting general locomotion and anxiety levels

(Fig. 5b-d, Supplementary Fig. 1g-h). Furthermore, the effect of 40 Hz blue light treatment and AQP4 inhibitor TGN020 on glymphatic drainage was evaluated by i.c.m. injection of Gd-DOTA followed by T1-weighted MRI (Fig. 5e). The results showed that 40 Hz blue light treatment induced a significant increase in Gd-DOTA perfusion rate in

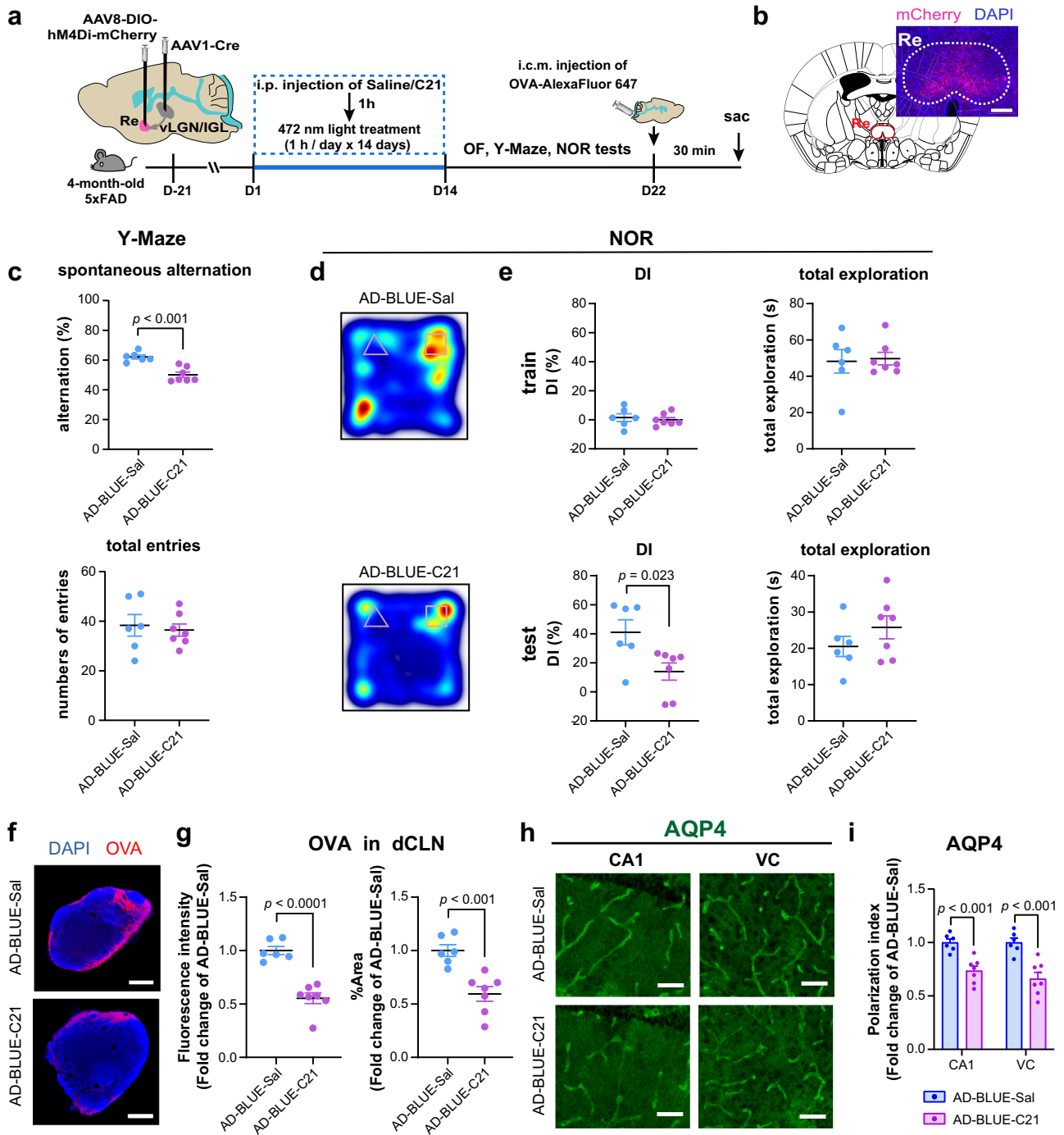


Fig. 3 | Inhibition of the vLGN/IGL-Re circuit blocks the effects of 40 Hz blue light treatment. **a** The experimental timeline of AAV infusion, C21 injections, blue light treatment, behavioral tests, injection of the OVA-Alexa Fluor 647 tracer into the cisterna magna (i.c.m.), and sacrifice (sac). **b** A representative image of hM4Di-mCherry expression in Re neurons receiving inputs from the vLGN/IGL projection. Red: mCherry; blue: DAPI; scale bar: 200 μ m. Two biological replicates of animal cohorts were performed with similar results. **c** The spontaneous alternation and total numbers of arm entries in the Y-maze test ($n = 6, 7$). **d** Representative heat-maps of animals' traveling paths during the test session of the novel object recognition (NOR). **e** Quantification of the discrimination index (DI) and the total time spent on exploring both objects (total exploration) during the training and the

test sessions of NOR ($n = 6, 7$). **f** Representative images depicting OVA tracer (red) and DAPI staining (blue) in the deep cervical lymph nodes (dCLNs). Scale bar, 250 μ m. **g** Quantification of the fluorescence intensity and the percentage of area covered by the OVA tracer in the dCLNs ($n = 6, 7$). **h** Representative images of AQP4 staining in cornu ammonis 1 (CA1) and the primary visual cortex (VC). Scale bars, 50 μ m. **i** Quantification of the polarization index of AQP4 in CA1 and VC ($n = 6, 7$). AD-BLUE-Sal, 5xFAD mice that received blue light treatment and saline injection; AD-BLUE-C21, 5xFAD mice that received blue light treatment and C21 injection. All data are presented as the mean \pm SEM and analyzed by two-tailed unpaired Student's *t* test.

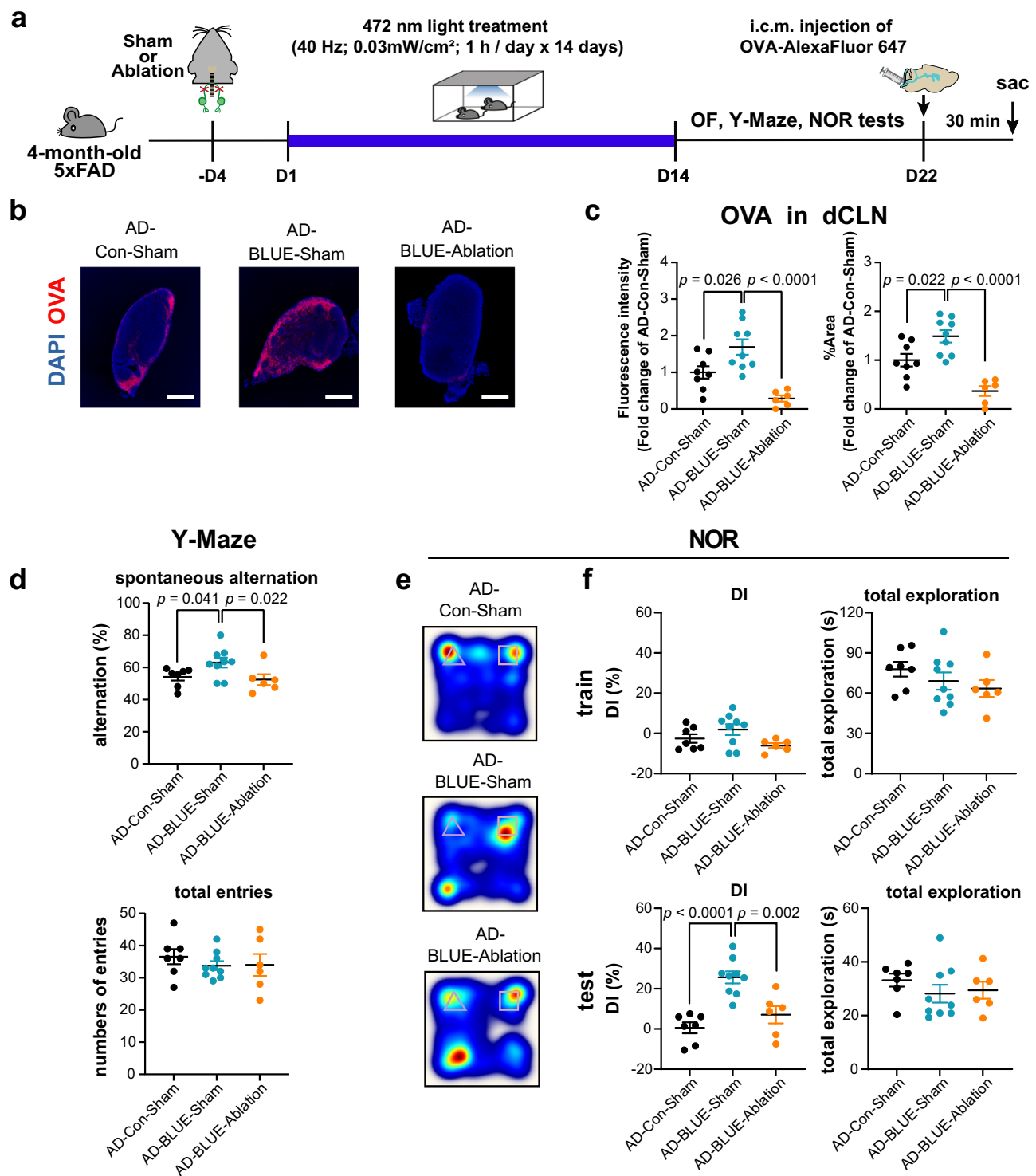
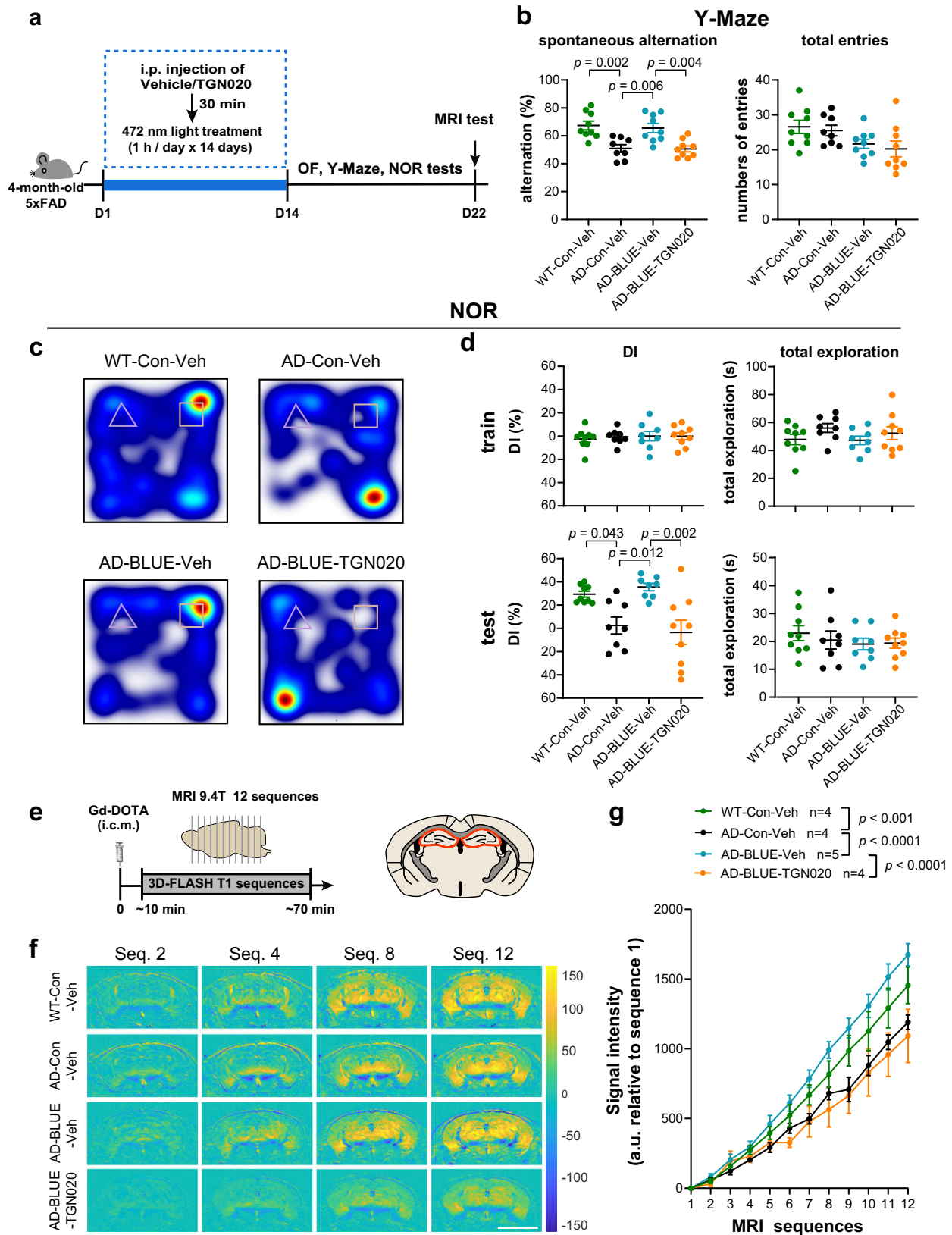


Fig. 4 | Blockade of brain drainage pathway prevents the effects of 40 Hz blue light treatment. **a** The experimental timeline of the surgical ablation of the lymphatic afferent vessels to the deep cervical lymph nodes (dCLNs), blue light treatment, behavioral tests, injection of the OVA-Alexa Fluor 647 tracer into the cisterna magna (i.c.m.) and sacrifice (sac). **b** Representative images depicting OVA tracer (red) and DAPI staining (blue) in the dCLNs. Scale bar, 250 μ m. **c** Quantification of the fluorescence intensity and the percentage of area covered by the OVA tracer in the dCLNs ($n = 8, 9, 6$). **d** The spontaneous alternation and total numbers of arm entries in the Y-maze test ($n = 7, 9, 6$). **e** Representative heatmaps of animals' traveling paths during the test session of the novel object recognition

(NOR). **f** Quantification of the discrimination index (DI) and the total time spent on exploring both objects (total exploration) during the training and the test sessions of NOR ($n = 7, 9, 6$). AD-Con-Sham, 5xFAD mice that did not receive blue light treatment and lymphatic vessel ablation; AD-BLUE-Sham, 5xFAD mice that received blue light treatment but did not receive lymphatic vessel ablation; AD-BLUE-Ablation, 5xFAD mice that received blue light treatment and lymphatic vessel ablation. All data are presented as the mean \pm SEM and analyzed by one-way ANOVA followed by Tukey's (c, f, d, total entries) or Fisher's LSD (d, spontaneous alteration) *post hoc* tests.



the hippocampus of 5xFAD mice, an effect which was abrogated by co-treatment with TGN020 (Fig. 5f-g).

Collectively, these results suggest AQP4 function is required for the improvement in glymphatic and cognitive functions mediated by 40 Hz blue light treatment.

Blue light treatment decreases lipid accumulation in the hippocampus of 5xFAD mice

Previous studies have reported contradictory findings regarding whether 40 Hz light stimulation could modulate microglia activity or A β plaque load in the mouse models of AD pathology¹⁴⁻¹⁶. In this study,

Fig. 5 | Suppression of AQP4 function mitigates the effects of 40 Hz blue light treatment. **a** The experimental timeline of the TGN020 injection, blue light treatment, behavioral tests, magnetic resonance imaging (MRI) test and sacrifice (sac). **b** The spontaneous alternation and total numbers of arm entries in the Y-maze test ($n = 9, 8, 9, 9$). **c** Representative heatmaps of animals' traveling paths during the test session of the novel object recognition (NOR). **d** Quantification of the discrimination index (DI) and the total time spent on exploring both objects (total exploration) during the training and the test sessions of NOR ($n = 9, 8, 8, 9$). **e** Schematic of MRI test. **f** Representative images of Gd-DOTA signal intensity gain

in MRI sequences. Scale bar, 3 mm. **g** Quantification of the Gd-DOTA signal intensity gain (relative to baseline) in the hippocampus over 12 MRI acquisition sequences ($n = 4, 4, 5, 4$). WT-Con-Veh, wild-type littermates that did not receive blue light treatment and injected with vehicle; AD-Con-Veh, 5xFAD mice that did not receive blue light treatment and injected with vehicle; AD-BLUE-Veh, 5xFAD mice that received blue light treatment and vehicle injection; AD-BLUE-TGN020, 5xFAD mice that received blue light treatment and TGN020 injection. All data are presented as the mean \pm SEM and analyzed by one-way ANOVA (**b, d**) or two-way ANOVA (**g**) followed by Tukey's *post hoc* tests.

we found that blue light treatment had limited effects on microglia activation, as the soma size of ionized calcium binding adapter molecule 1 (IBA1)-labeled microglia, the fluorescent intensity, and coverage area of IBA1 staining remained largely unchanged following blue light treatment, with the exception of a reduction in soma size observed in the CA1 subregion of hippocampus (Supplementary Fig. 9a-b). Similarly, the fluorescent intensity and coverage area of the phagocytotic marker CD68 within IBA1-labeled microglia were mostly unaltered in the hippocampus and VC by blue light treatment, except for a reduction in the CA1 subregion of hippocampus (Supplementary Fig. 9c-d). Furthermore, the primary process length of microglia as well as the percentage of microglia co-localized with A β in the cell body was not affected by the blue light treatment (Supplementary Fig. 9e-h). Additionally, blue light treatment exhibited limited effects on A β deposit density and coverage area, with only a reduction in the A β covered area noted in the hippocampal CA1 subregion of 4-month-old 5xFAD mice (Supplementary Fig. 10a-b).

The glymphatic system is responsible for the transport of brain lipids, and disruptions in such transport can lead to lipid accumulation and pathological alterations in astrocytes⁴⁴. Considering the reported alterations in lipidomic profiles observed in AD patients⁴⁵⁻⁴⁸, we performed an unbiased lipidomic analysis and compared lipid profiles in the hippocampus of 5xFAD mice with and without 40 Hz blue light treatment, alongside wild-type littermate controls (Supplementary Fig. 11a). Partial least squares discrimination analysis (PLS-DA) showed separation among the three groups of wild-type, 5xFAD, and 5xFAD with blue light treatment (Supplementary Fig. 11b). Notably, compared to wild-type mice, the 5xFAD mice without light treatment exhibited significant increases in various lipid species, whereas 40 Hz blue light treatment resulted in significant decreases in lipid species in the hippocampus of 5xFAD mice (Supplementary Fig. 11c). Cross-examination yielded 217 differentially expressed lipids shared by comparisons of wild-type versus 5xFAD mice and 5xFAD mice with versus without light treatment (Supplementary Fig. 11d-e). Notably, 5xFAD mice exhibited large increases in several lipid species, including phosphatidylcholines (PCs), triacylglycerols (TAGs), and phosphatidylethanolamines (PEs) in the hippocampus when compared with wild-type group. Importantly, these elevated levels were mitigated following 14-day 40 Hz blue light treatment (Supplementary Fig. 11f).

These data, along with our previous findings of reduced soluble A β 42 level, suggest that 40 Hz blue light treatment may enhance the clearance of lipids and soluble A β 42 from the hippocampus through improved glymphatic drainage function in 5xFAD mice.

Blue light treatment enhances motivative behaviors and glymphatic drainage in 14-month-old 5xFAD mice

To further investigate the potential therapeutic benefits of low-intensity 40 Hz blue light on middle to late-stage AD-related pathology and behavioral changes, we administered the same 0.03 mW/cm² 40 Hz blue light treatment to 14-month-old 5xFAD mice for 1 h per day over a period of 14 days (Fig. 6a). Of note, while memory loss is a well-known early symptom of AD, apathy or loss of motivation is also commonly observed in AD patients⁴⁹. Here, we found that 14-month-old 5xFAD mice, compared to their wild-type

littermates, exhibited significantly reduced exploration of the Y-maze arms, and spent less time exploring objects or interacting with a novel mouse in the novel object recognition and social interaction tests (Fig. 6b-m). Interestingly, the blue light treatment significantly improved motivational behaviors in these 5xFAD mice (Fig. 6b-m).

Similar to observations in 4-month-old 5xFAD mice, 40 Hz blue light treatment notably enhanced the perfusion of intracisternally-injected OVA-AF647 tracer into the brain parenchyma and improved the clearance of the tracer into the dCLNs in 14-month-old 5xFAD mice (Fig. 7a-d). Immunofluorescence staining showed that the disruption of perivascular distribution of AQP4 in the hippocampus and VC of the 14-month-old 5xFAD mice was also significantly reversed by blue light treatment (Fig. 7e-f). Correlation analyses revealed significant correlations between clearance of intracisternally-injected OVA-AF647 tracer into the dCLNs and AQP4 polarity levels in the hippocampus or VC for the 14-month-old 5xFAD mice, as well as a weak correlation in the 4-month-old 5xFAD mice, suggesting a link between AQP4 polarity alterations and glymphatic system functionality (Supplementary Fig. 12). Of note, similar to 4-month-old 5xFAD mice, blue light treatment also exhibited limited effects on A β deposit density and coverage area in 14-month-old 5xFAD mice, with only a reduction in immunofluorescence density noted in the hippocampal CA3 subregion (Supplementary Fig. 10c-d).

Collectively, these data demonstrate that 40 Hz blue light treatment effectively improves motivational behaviors and increases glymphatic drainage in the 14-month-old 5xFAD mice.

Blue light treatment enhances the efficacy of anti-A β immunotherapy on cognitive improvement and soluble A β reduction

Lecanemab, an antibody that binds to A β soluble oligomers and protofibrils with high affinity, has been recently demonstrated to prevent cognitive decline in early-stage AD patients and thus has received approval for clinical use. However, the administration of lecanemab carries the risk of serious adverse events, such as ARIA in a dose-dependent manner⁴. To investigate whether blue light treatment could improve the efficacy of anti-A β immunotherapy, we combined blue light treatment with a single intracisternal injection of a low-dose mAb158 (the murine version of lecanemab) into the CSF of 4-month-old 5xFAD mice (Fig. 8a). The results showed that while the low-dose mAb158 alone led to an improvement in spatial working memory as assessed by the Y-maze in 5xFAD mice, no significant change was observed for long-term object recognition memory (Fig. 8b-d). The combination of 40 Hz blue light treatment significantly augmented the effects of mAb158 in enhancing long-term object recognition memory (Fig. 8c, d). Neither blue light treatment nor mAb158 administration had a notable effect on anxiety-like behaviors or general locomotion in the open field test (Supplementary Fig. 1i-j). Furthermore, the combination of blue light treatment with anti-A β immunotherapy effectively reduced soluble A β 42 levels in the hippocampus of 5xFAD mice (Fig. 8e). However, there was no significant change in the A β deposit density and coverage area (Supplementary Fig. 10e, f).

Taken together, these results suggest that blue light treatment enhances the effect of anti-A β immunotherapy on cognitive improvement and soluble A β clearance in 5xFAD mice.

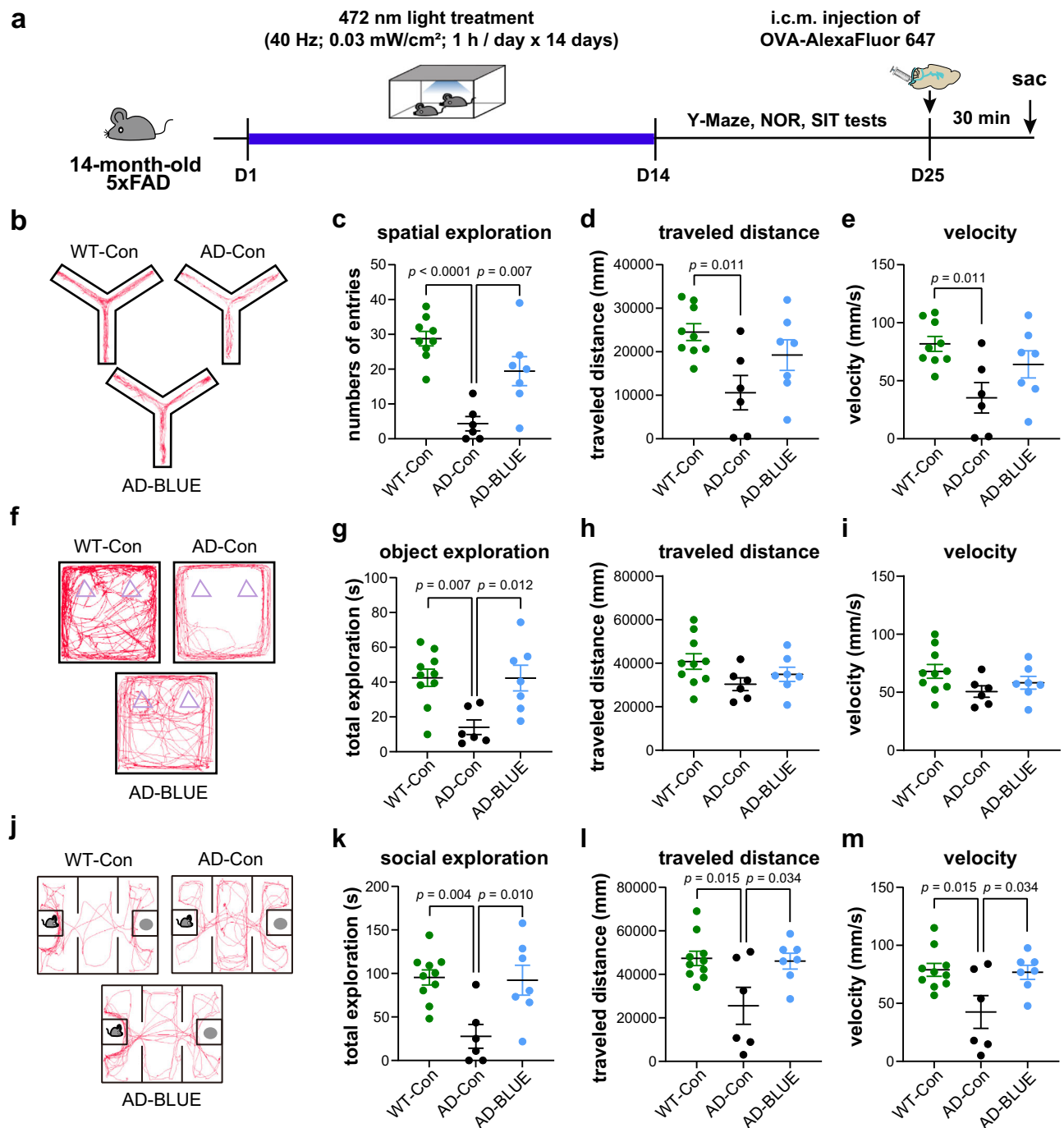


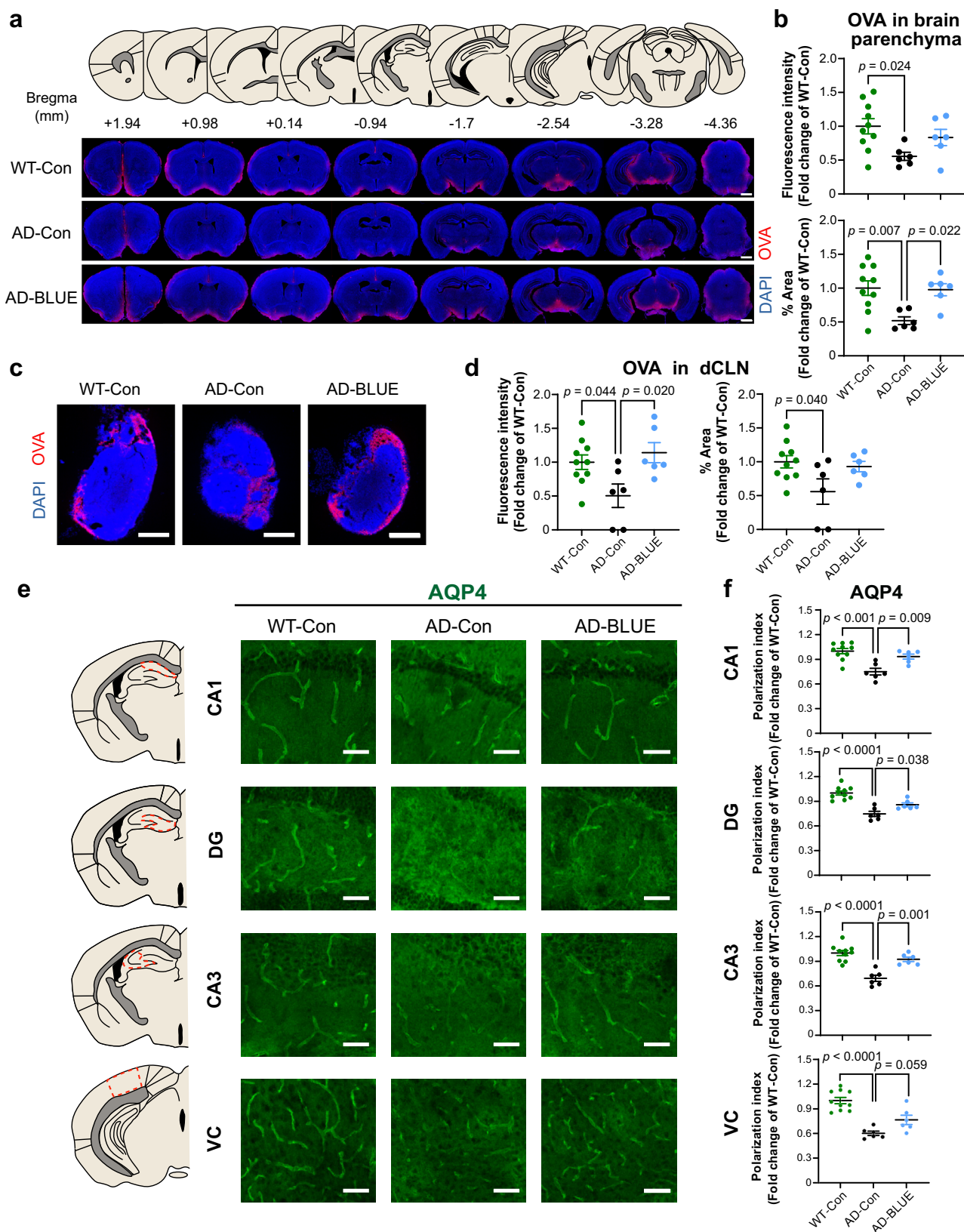
Fig. 6 | 40 Hz blue light treatment enhances motive behaviors in 14-month-old 5xFAD mice. **a** The experimental timeline of blue light treatment, behavioral tests, injection of the OVA-Alexa Fluor 647 tracer into the cisterna magna (i.c.m.) and sacrifice (sac). **b** Representative traces of animals' traveling paths in the Y-maze. **c** The total numbers of arm entries in the Y-maze test ($n = 9, 6, 7$). **d** Quantification of the total traveled distance in the Y-maze test ($n = 9, 6, 7$). **e** Quantification of the velocity in the Y-maze test ($n = 9, 6, 7$). **f** Representative traces of animals' traveling paths during the training session of the novel object recognition (NOR). **g** Quantification of the total time spent on exploring both objects during the training sessions of NOR ($n = 10, 6, 7$). **h** Quantification of the total traveled distance

in the NOR training session ($n = 10, 6, 7$). **i** Quantification of the velocity in the NOR training session ($n = 10, 6, 7$). **j** Representative traces of animals' traveling paths in the social interaction test (SIT). **k** Quantification of the total time spent on exploring the social subject (a novel mouse) and the non-social subject (a toy mouse) during the SIT ($n = 10, 6, 7$). **l** Quantification of the total traveled distance in the SIT ($n = 10, 6, 7$). **m** Quantification of the velocity in the SIT ($n = 10, 6, 7$). WT-Con, wild-type littermates that did not receive blue light treatment; AD-Con, 5xFAD mice that did not receive blue light treatment; AD-BLUE, 5xFAD mice that received 40 Hz blue light treatment. All data are presented as the mean \pm SEM and analyzed by one-way ANOVA followed by Tukey's *post hoc* test.

Discussion

In summary, our study demonstrates that exposing an early-stage β -amyloidopathy mouse model for AD to low-intensity 40 Hz blue light for 1 h daily over 14 days effectively restores AQP4 polarity, enhances glymphatic drainage efficiency, and significantly improves memory

performance that is functionally dependent on the vLGN/IGL-Re circuit and AQP4. Furthermore, our results reveal that this treatment also restores motivation and glymphatic function in middle-to-late-stage β -amyloidopathy mice. Additionally, our data suggest that in combination with blue light, the anti-A β immunotherapy regimen shows



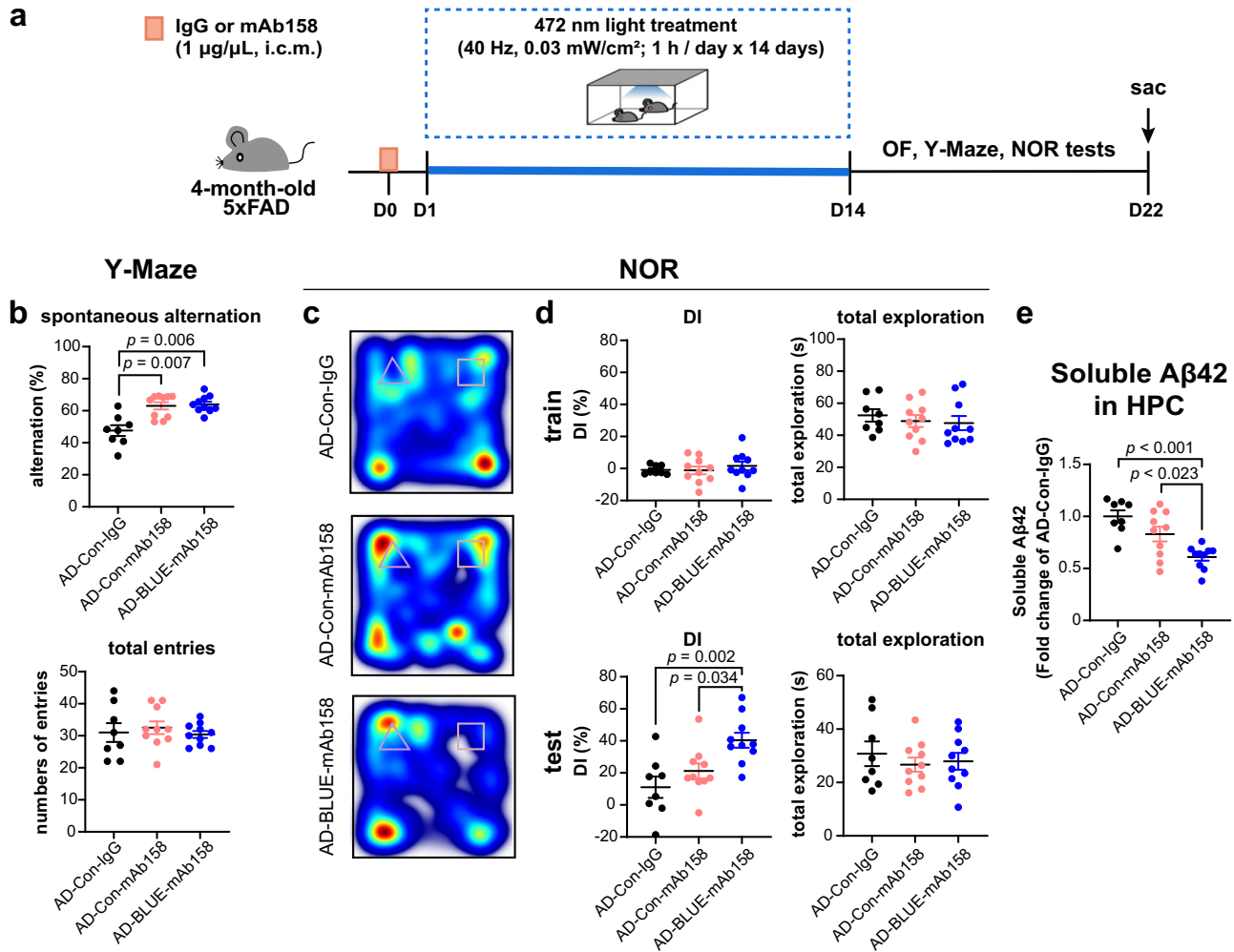
increased effectiveness for its cognitive benefit and soluble A β 42 clearance. Overall, these findings offer functional evidence on the efficacy of blue light therapy as a non-invasive intervention for A β -related pathology and cognitive impairment.

Compared to drugs and other electromagnetic physical interventions, light therapy offers the advantages of being non-invasive,

relatively safe, and easy to use^{50,51}. Numerous clinical studies over the past decades have explored white light therapy in AD and other neuropsychiatric conditions^{51–53}. However, previous studies using white light have presented challenges in evaluating, standardizing, and optimizing light therapy conditions due to its mixed nature and varying physical parameters. Furthermore, it is widely accepted that

Fig. 7 | 40 Hz blue light treatment increases glymphatic drainage in 14-month-old 5xFAD mice. **a** Upper panel, the atlas of the brain coronal sections collected. Lower panel, representative images depicting intracisternally-injected OVA tracer (red) distribution. The sections were counterstained with DAPI (blue). Scale bar, 1000 μm . **b** Quantification of the fluorescence intensity and the percentage of area covered by the OVA tracer in the brain parenchyma ($n = 10, 6, 6$). **c** Representative images depicting OVA tracer (red) and DAPI (blue) staining in the deep cervical lymph nodes (dCLNs). Scale bar, 250 μm . **d** Quantification of the fluorescence intensity and the percentage of area covered by the OVA tracer in the dCLNs ($n = 10,$

6, 6). **e** Representative images of the immunofluorescence staining of AQP4 in the cornu ammonis 1 (CA1), dentate gyrus (DG) and cornu ammonis 3 (CA3) subregions of the dorsal hippocampus and the primary visual cortex (VC). Scale bars, 50 μm . **f** Quantification of the polarization index of AQP4 across different brain regions ($n = 10, 6, 6$). WT-Con, wild-type littermates that did not receive blue light treatment; AD-Con, 5xFAD mice that did not receive blue light treatment; AD-BLUE, 5xFAD mice that received 40 Hz blue light treatment. All data are presented as the mean \pm SEM and analyzed by one-way ANOVA followed by Tukey's *post hoc* test.



ELISA ($n = 8, 10, 10$). AD-Con-IgG, 5xFAD mice that did not receive blue light treatment and received control IgG injection; AD-Con-mAb158, 5xFAD mice that did not receive blue light treatment and received mAb158 injection; AD-BLUE-mAb158, 5xFAD mice that received blue light treatment and mAb158 injection. All data are presented as the mean \pm SEM and analyzed by Kruskal–Wallis test with Dunn's *post hoc* test (**b**, spontaneous alteration; **d**, train DI and train total exploration) or one-way ANOVA followed by Tukey's *post hoc* test (**b**, total entries; **d**, test DI and test total exploration; **e**).

white light come into effect at a relatively high-intensity, which may lead to side effects such as increased heat production, potentially causing discomfort to patients^{54–56}.

Previous studies have shown that ipRGCs, rather than rod or cone cells, play a critical role in light-mediated regulation of cognition and mood. The ipRGCs exhibit the highest sensitivity to blue light⁵⁷. When activated by light, ipRGCs transmit information via the optic nerve to the vLGN/IGL, which in turn projects to the key brain areas involved in

processing cognition and emotion^{41,58}. In this study, we demonstrated that a relatively low intensity of blue light treatment could effectively enhance spatial working memory and long-term object memory in the early-stage 5xFAD mice. We noticed that in the 5xFAD mice, the functional activity of the VC and SC, brain regions related to the visual pathway, was reduced, but was enhanced by blue light treatment. Furthermore, light therapy reversed the decreased functional activity in cognition-related brain regions including the hippocampus, the Re,

and the retrosplenial cortex. These improvements may contribute to the cognitive enhancement observed in 5xFAD mice following light therapy. Indeed, Re neurons receive retinal input from the vLGN/IGL projection, which can be activated by high intensity light treatment to promote spatial memory formation in wild-type mice⁴¹. However, it is worth noting that the same light treatment failed to promote spatial memory in 6-month-old 5xFAD mice⁴¹. On the other hand, we showed that low-intensity 40 Hz blue light treatment can effectively improve the cognitive function in 4-month-old 5xFAD mice, suggesting the frequency instead of intensity of light treatment may play a critical role in mediating the cognitive improvement in 5xFAD mice.

Our findings revealed that 40 Hz blue light treatment significantly increased the activity of vLGN/IGL-Re projection, which in turn mediates the light-induced improvement in cognitive function, glymphatic drainage and restoration of AQP4 polarity in the hippocampus and VC, likely through direct projection from the vLGN/IGL-Re circuit to these two brain regions. Importantly, suppression of the vLGN/IGL-Re pathway reversed the beneficial effect of 40 Hz blue light treatment on AQP4 polarity in CA1 and VC brain areas, while activation of this pathway was sufficient to increase AQP4 polarity in these two brain regions of 5xFAD mice. These data suggest a previously overlooked role of the visual circuit in regulating AQP4 polarity in astrocyte endfeet.

How this pathway mediates the improvement of glymphatic activity remains underexplored. It is noteworthy that a recent investigation revealed that a short 30-min exposure to 40 Hz white light augments glymphatic drainage via elevating adenosine release, thereby modulating vasomotion in the cerebral cortex and AQP4 polarity⁵⁹. Global knockout of the adenosine transporter, equilibrative nucleoside transporter 2 (ENT2), and the adenosine receptor A2AR, both led to the abrogation of the acute increase in vasomotion, AQP4 polarity, and glymphatic drainage induced by 40 Hz white light⁵⁹. The heightened adenosine release in the brain might be attributable to increased neuronal activity stimulated by light, suggesting a functional connection between light-regulated neural circuit activity and adenosine release in modulating the brain's glymphatic system. Further mechanistic studies are warranted to investigate how blue light received by ipRGCs activates vLGN/IGL-Re pathway to regulate astrocyte activation and the perivascular distribution of AQP4, leading to improved functionality of glymphatic system.

Prior research has suggested that 40 Hz white light flickers, compared to steady light or other frequencies, are more effective in enhancing cognitive functions in the mouse models of AD pathology^{14,15,60}. A recent study has also reported that 40 Hz blue light, in comparison to constant blue light, leads to greater changes in hippocampal activation and its functional connectivity⁶¹. However, there are conflicting reports regarding the underlying mechanisms. While initial studies suggest that 40 Hz light therapy induces gamma oscillations, decreases A β plaques, and suppresses microglial activation, these findings have been contested by later investigations^{15,16}. Our study also revealed limited effects of 40 Hz blue light treatment in reducing A β deposits and microglia activation, indicating that the positive impact of 40 Hz blue light treatment on cognitive enhancement in 5xFAD mice may not operate through these mechanisms. The glymphatic system is a crucial pathway for clearing toxic molecules, including A β , from the ISF of brain^{38,62}. Our study also revealed a significant reduction in hippocampal soluble A β 42, alongside with the beneficial effects of 40 Hz blue light on glymphatic drainage and cognitive function in 5xFAD mice. Importantly, prior research has suggested that soluble A β 42 contributes to synaptic deficits and subsequent cognitive dysfunction in mouse models of AD pathology⁶³. Therefore, our findings suggest that the enhancement of glymphatic function by blue light treatment may facilitate the clearance of soluble A β 42 from the 5xFAD mouse brain, thereby reducing its synaptic toxicity and ultimately leading to improved behavioral outcomes.

The approach employed to directly impair the outflow of the glymphatic system—specifically, the ligation of afferent lymphatic vessels to dCLNs, has been previously documented, which have demonstrated that directly obstructing the glymphatic outflow to dCLNs does not alter cognitive function in wild-type mice. However, it significantly impacts the pathology of AD-related mouse models, manifesting in more severe cognitive deficits and exacerbated amyloidopathy^{64,65}. Our data demonstrate that 40 Hz blue light treatment facilitates the clearance of soluble A β 42, which may slow down the plaque deposition rate, a long process involving imbalanced production and clearance^{66,67}. As a result, a prolonged duration of light exposure may be necessary to substantially reduce A β deposits.

The glymphatic system is also known for the transport of brain lipids, and disruptions in such transport can lead to lipid accumulation and pathological alteration of astrocytes⁴⁴. Previous study has reported alterations in lipidomic profiles in AD patients^{45–48}. Our results now revealed that 40 Hz blue light treatment mitigated the increase in various lipid species including PCs, PEs, and TAGs in the hippocampus of 5xFAD mice. Notably, the peroxidation of phospholipids and fatty acids have been reported as a driving force behind mitochondrial dysfunction and ferroptosis^{68–71}. Impairment in glymphatic clearance may redirect lipid metabolism from clearance towards accumulation, thereby exacerbating lipid stress and associated cellular pathologies in neurons and glia. Our study suggests that enhanced drainage of the glymphatic system by blue light may facilitate lipid clearance, thus preventing the detrimental effects of lipid stress in the brains of 5xFAD mice.

Since its discovery in 2012, the impact of glymphatic drainage impairment on the progression of AD and other neuropsychiatric disorders has garnered significant attention^{17,72–75}. However, approaches to modulate glymphatic drainage efficiency remain underexplored. Recent studies have shown that checkerboard visual stimulation can expedite paravascular clearance in mice and promote widespread CSF flow in the human brain, suggesting regulation of glymphatic function by visual pathways^{25,26}. Our research demonstrates that 40 Hz blue light treatment enhances the perfusion and clearance of CSF tracer, potentially through restoring the perivascular localization of astrocytic water channel AQP4, proposing 40 Hz blue light treatment as a non-invasive method to improve glymphatic function. Importantly, we performed functional manipulation to show that the restoration of AQP4 function was required for the improvement in brain drainage and cognitive function by blue light treatment in 5xFAD mice. It is worth pointing out that alterations in glymphatic drainage are not exclusive to AD, but also common in other neurodegenerative diseases, brain injuries and neuropsychiatric disorders^{76,77}. Our findings suggest that 40 Hz blue light therapy may provide therapeutic benefits for this series of diseases.

Previous animal models and clinical studies of AD have primarily focused on repairment on memory function^{55,78}. However, nearly half of AD patients experience apathy, characterized by a loss of motivation, with a higher incidence as the disease progresses. Apathy has been linked to reduced quality of life and higher morbidity rates in AD patients as well as increased caregiver distress^{79,80}. Limited evidence supports the efficacy of psychotropic drugs, such as antidepressants, in treating apathy in AD patients, with some studies even suggesting that these drugs may exacerbate symptoms⁸¹. Our study revealed that 14-month-old 5xFAD mice, in comparison to their wild-type counterparts, displayed motivation loss-like symptoms similar to those seen in human patients, which were effectively reversed by 40 Hz blue light therapy. The behavioral improvements were accompanied by an increase in glymphatic drainage. These findings indicate that blue light therapy not only enhances cognitive functions in young 5xFAD mice, but also effectively alleviates AD-related motivational behavioral abnormalities in aged 5xFAD mice. Of note, while Y-maze and novel object recognition tests were conducted on mice at both ages,

different behavioral phenotypes were observed. The 4-month-old 5xFAD mice exhibited memory deficits that were alleviated by blue light treatment, but showed no apathy-like behaviors. In the 14-month-old 5xFAD mice, a pronounced absence of motivation indicating apathy was detected, which impeded the assessment of memory performance in these tests, as they rely on animals' exploratory behaviors during training.

Recently, lecanemab has demonstrated effectiveness in reducing brain amyloid levels and slowing cognitive decline in AD patients, leading to its approval for clinical use in the United States, Japan, and China⁸². However, findings from clinical trials have highlighted dose-related effects of lecanemab in increasing the incidence of ARIA⁸². At its effective dose, the incidence of ARIA-related edema with lecanemab treatment was 9.9%, compared to 0.8% for placebo⁴. Another limitation of lecanemab is the high cost associated with repeated administration⁸³. Our study showed that the combined use of low-dose mAb158, a murine version of lecanemab, and 40 Hz blue light treatment significantly increased soluble A β 42 clearance and cognitive functions in 5xFAD mice. These findings suggest the potential of 40 Hz blue light treatment as an adjunctive therapy to increase the clinical effectiveness of anti-A β immunotherapy, potentially reducing the required antibody dose and thereby decreasing the occurrence of immunotherapy-related adverse events while easing financial burdens on patients' families.

During the preparation of this manuscript, a study using multisensory audio-visual 40 Hz stimulation was reported to increase glymphatic drainage in 6-month-old 5xFAD mice⁸⁴. However, the long-term effects of 40 Hz light stimulation to 5xFAD mice have not been examined. Our findings now showed that by applying relatively low-intensity 40 Hz blue light stimulation, a significant improvement in mental functions and accelerated glymphatic drainage were shown in both young and middle age 5xFAD mice. However, unlike the report from multisensory 40 Hz treatment, we found limited effects on meningeal lymphatic vessels, microglia activation and A β deposits in 5xFAD mice that received 40 Hz blue light treatment, suggesting different mechanisms may exist. Our data also indicate that 40 Hz blue light treatment may enhance glymphatic drainage, thereby promoting the clearance of various toxic molecules, such as soluble A β and lipids. This, in turn, might have a positive impact on cognitive functions in 5xFAD mice.

It is important to acknowledge the limitations of this study. First, the mechanisms underlying the regulation of the glymphatic system by 40 Hz blue light treatment and its associated visual circuits remain underexplored, which is warranted for further investigation. Second, although our findings indicate that 40 Hz blue light treatment reduces soluble A β levels and lipid stress in the hippocampus of 5xFAD mice through enhanced glymphatic function, the precise mechanisms through which these changes lead to cognitive improvements remain to be elucidated. Additionally, our results do not rule out potential off-target effects resulted from the systemic administration of TGN020, which may not only inhibit AQP4 function in the brain but also alter AQP4 and other aquaporin proteins in peripheral tissues, potentially disrupting systemic water regulation and electrolyte homeostasis. Chronic inhibition of AQP4 by TGN020 may also disrupt the physiological roles and metabolic support provided by astrocytes, leading to changes in neuronal activity and synaptic plasticity, which ultimately impact cognitive performance⁸⁵.

To summarize, our findings reveal that low-intensity 40 Hz blue light treatment enhances glymphatic drainage and cognitive performance that are functionally associated with the vLGN/IGL-Re circuit and AQP4. The same treatment also improves motivation and glymphatic function in the middle age 5xFAD mice. Furthermore, the combination of anti-A β immunotherapy with 40 Hz blue light treatment exhibits increased effects than immunotherapy alone in alleviating cognitive impairment and reducing soluble A β 42. Collectively,

our findings highlight the therapeutic potential and safety of low-intensity 40 Hz blue light treatment and as the adjunctive therapy of anti-A β immunotherapy for patients with dementia.

Methods

Animals

All animal procedures were approved by the Institutional Animal Care and Use Committee of the Sun Yat-sen University (approval number: SYSU-IACUC-2022-001564). 5xFAD mice were initially obtained from the Jackson Laboratory (JAX: 034840) with a B6/SJL genetic background, and has undergone more than 10 generations of backcrossing to the C57BL/6J background. Female and male 5xFAD mice aged 4 and 14 months, along with their wild-type littermates, were used in this study. For the investigation of light treatment's effect on the efflux of intraparenchymally injected OVA-AF647, female and male wild-type C57BL/6J mice aged 4 months were obtained from Zhuhai Bai Shi Tong Animal Center (Zhuhai, China). All animals were housed in a Specific-Pathogen-Free (SPF) animal facility with controlled temperature (23 ± 2 °C) and humidity (50–60%), following a standard 12-h light/dark cycle. Food and water were provided *ad libitum*. Prior to experiments, the animals underwent a minimum of 1-week habituation period in the facility, and were randomly assigned to different experimental groups.

Light treatment

Blue light-emitting diode (LED) devices with a centroid wavelength of 472 nm, a time modulation frequency of 40 Hz (12.5 ms light on, 12.5 ms light off), and an irradiation power density of 0.03 mW/cm² (illumination intensity of 160–180 lux) were utilized in the experiments. These devices were installed at the top of test cages measuring 25 cm in length, 20 cm in width and 25 cm in height. The animals in both the control and light treatment groups were transferred to these cages at 9 a.m. for 14 consecutive days. Each day, mice in the light treatment group were exposed to 1 h of 40 Hz blue light, while the control mice stayed in the cages without blue light exposure. The light exposure procedure was performed under dim room light (~50 lux).

Behavioral paradigms

The mice were handled for four days before the start of behavioral experiments. Behavioral tests were performed during the light phase (1 p.m. to 7 p.m.) in a quiet room with dim lighting. Prior to each test, the animals were given 1–2 h to acclimate to the testing environment. The behavioral testing apparatus was cleaned with 75% ethanol between each trial.

Open field test. Exploratory behaviors were measured in a light blue PVC box (40 × 40 × 40 cm). The mice were placed in the center of the box and allowed to explore the arena for 10 min. The total distance of the exploration, as well as the distance and time spent in the 20 × 20 cm center zone of the arena was recorded and analyzed by the TopScan software (CleverSys Inc., Reston, VA, USA) to evaluate locomotor activity and the anxiety-like behaviors.

Novel object recognition test. The mice were habituated to the experimental room and apparatus for three consecutive days prior to training. During the habituation sessions, the mice were allowed to freely explore the blue box (40 × 40 × 40 cm) without any object for 10 min each day. On the training day, the mice explored the same arena for 10 min with two identical objects placed on the two ends 10 cm away from a side wall. During the testing phase, 24 h after training, the mice were evaluated for their long-term object recognition memory over a 5-min period, with one of the original objects replaced by a novel object while maintaining the position of the objects. Both phases were videotaped. The time spent exploring the objects were analyzed by an investigator blinded to the experimental groups. Animals that spent <20 s exploring objects during the training session or <10 s

exploring objects during the test session were excluded from further analysis. One animal was excluded due to this reason. The traveled distance and velocity of the exploration, as well as heatmaps or traces of animals' traveling paths, were analyzed and generated by the EthoVision XT software (version 15.0.1416, Noldus, Netherlands). The discrimination index (DI %) was calculated as follows: (the time spent exploring the novel object—the time spent exploring the familiar object) / (the time spent exploring both objects) × 100%. The DI % for the testing phase was used to determine the animals' memory capacity.

Y-Maze test. The Y-Maze task was utilized to assess working memory through the measurement of spontaneous alternation. The mice were placed in the center of the Y-Maze, consisting of 3 arms that were 50 cm in length, 10 cm in width and 20 cm in height, and allowed to freely explore for 5 min. The test was videotaped. The arm entries were analyzed by an investigator blinded to the experimental groups. Heatmaps or traces of animals' traveling paths were generated by the EthoVision XT software (version 15.0.1416, Noldus, Netherlands). An arm entry was considered complete when the hind paws of the mouse had fully entered the arm. A correct spontaneous alternation event was defined as the completion of sequential entries into three different arms. The percentage of correct alternation (Alternation %) was calculated as follows: (the number of correct alternations) / (the number of total entries - 2) × 100. Alternation % was used to determine the animals' working memory capacity.

Social interaction test. The test was conducted using a white PVC box measuring 60 cm in length, 40 cm in width, and 20 cm in height, with three distinct transparent chambers. Two wire-mesh enclosures were placed in the middle of two outer chambers. A stranger C57BL/6J wild-type mouse was allowed to acclimate in one of the enclosures for 10 min the day before testing. On the day of testing, the subject mouse was placed in the middle chamber and allowed to explore the entire box with empty enclosures for 10 min. Subsequently, the stranger mouse was introduced into one enclosure, while a toy mouse was placed in the other. The subject mouse was then allowed to freely explore for an additional 10 min. Animal behaviors were videotaped and analyzed offline by an investigator blinded to the experimental conditions. Traces of animals' traveling paths were generated by the EthoVision XT software (version 15.0.1416, Noldus, Netherlands).

Intra-cisterna magna injection

For tracer injection, mice were anesthetized with intraperitoneal (i.p.) injection of sodium pentobarbital (100 mg/kg body weight). The eyes were lubricated with Vaseline mixed with sterile saline, and the mouse's head was secured in a stereotaxic frame (RWD Life Science, China). The hair on the neck was shaved, and the underlying skin was cleaned with iodine. A small incision was made at the midline, and the muscle layers were retracted to expose the cisterna magna. The injection was performed using an infusion pump (Model R452, RWD Life Science, China) with a Hamilton syringe connected to a 33-gauge needle via a PE tube. 5 µL of Ovalbumin-Alexa Fluor 647 (OVA-AF647, Thermo Scientific, Waltham, MA, USA; 0.5% in artificial cerebrospinal fluid) was injected into the subarachnoid space at a rate of 1 µL/min. After injection, the needle was left in place for an additional 5 min to prevent backflow of cerebrospinal fluid. The neck skin was then sutured. All mice were kept anesthetized on a heating pad and perfusion-fixed at 20 min after removal of the injection needles. A total of 4 animals that died following deep anesthesia or had OVA leakage during intracisterna magna injection were excluded from analysis. Intracisternal Aβ antibody infusion was performed in a similar manner. One day before the blue light treatment, 5 µL of mouse mAb158 (Absolute Antibody, Wilton Center; 1 µg/µL in PBS) or the control mouse mlgG2B (MAB004, R&D System, USA) was injected⁸⁶. The mice were allowed to recover on a heating pad until fully awake.

Lymphatic vessel ablation

The mice were anesthetized with its head secured on a stereotaxic apparatus (RWD Life Science, China). The cisterna magna was exposed by retracting the skin and muscle layers of the back neck, followed by the injection of 5 µL of 40 kDa Dextran-Fluorescein (Thermo Scientific, Waltham, MA, USA; 0.01% in sterile PBS) into the brain CSF. Ablation was performed by exposing the front neck under a fluorescence stereomicroscope (SMZ18, Nikon, Japan) and using an electrocoagulation electrotome to ablate the collecting lymphatic vessels anterior to the bilateral dCLNs. The mice were then sutured and allowed to recover on a heating pad until fully awake. Mice were allowed to recover after the surgery for 4 days before receiving the blue light treatment.

AQP4 inhibition and magnetic resonance imaging (MRI)

To pharmacologically inhibit AQP4 function, TGN020 (TargetMol, cat#: T5102, 100 mg/kg, 20 mL/kg dissolved in 10% DMSO) was injected intraperitoneally 30 min prior to 40 Hz blue light treatment daily, while control animals received vehicle (10% DMSO) injection.

For evaluating glymphatic function, the influx rate of a CSF tracer was assessed by MRI acquisition and analysis⁶⁴. The mice were anesthetized with a mixture of tiletamine and zolazepam (Virbac, Alpes-Maritimes, France, 85 mg/kg, dissolved in 0.9% saline, i.p.) and xylazine (Huamu, Jilin, China, 10 mg/kg, dissolved in 0.9% saline, i.p.)⁸⁷, followed by i.c.m. injection of 5 µL of gadoterate meglumine (Gd-DOTA, Jiangsu Hengrui, 377 mg/mL, 1 µL/min). The mice were positioned in an MRI scanner (9.4 Tesla, Bruker Biospin, USA) and maintained under light anesthesia with isoflurane. Ten minutes after i.c.m. injection of Gd-DOTA, each mouse underwent MRI scanning from the olfactory bulb to the cerebellum. Post-contrast 3D T1-weighted Fast Low Angle Shot (FLASH) images were acquired with the following parameters: repetition time = 30 ms; echo time = 8 ms; number of averages = 1; number of repetitions = 12; scan time = 272.64 s per sequence; flip angle = 20°, field of view = 16 × 16 × 16 mm, matrix size 128 × 128 × 64, spatial resolution = 125 × 125 × 250 µm, slice thickness = 250 µm, number of slices = 64, using a 4-element RF ARR 400 1H M receiving coil. A total of 12 sequences were acquired per mouse. Data were analyzed using MicroDicom (version 2024.2, MicroDicom Ltd, Bulgarian), with manual identification of the dorsal hippocampus as the region of interest (ROI). Rate of contrast agent influx within the ROI was calculated by measuring the contrast agent signal intensity of each sequence, followed by subtracting the baseline intensity value (sequence 1) from the intensity value of each subsequent sequence. Representative images were made by MATLAB (version R2024a, MathWorks, USA).

Brain parenchymal injection

Mice were anesthetized and head-fixed on a stereotaxic frame (RWD Life Science, China). For tracer injection, striatum (A/P: +1.0 mm; M/L: ±1.5 mm; D/V: -3.5 mm) and hippocampus (A/P: -2.0 mm; M/L: ±1.5 mm; D/V: -2 mm) were injected with 200 nL Ovalbumin-Alexa Fluor 647 (Thermo Scientific, Waltham, MA, USA; 0.5% in artificial cerebrospinal fluid) at a rate of 40 nL/min, with the needle left in place for an additional 5 min before withdrawal. Mice were sacrificed 1 h after injection. For chemogenetic inhibition of Re neurons receiving vLGN/IGL projections, AAV1-hSyn-NLS-Cre (Braincase, cat#: BC-0159, 1.02E + 13 v.g./mL) was bilaterally injected into the vLGN/IGL (100 nL/side, AP: -2.4 mm; ML: ± 2.47 mm; DV: -3.4 mm) and AAV8-hSyn-DIO-hM4Di-mCherry (BrainVTA, cat#: PT-0020, 5.31E + 12 v.g./mL) was injected into the Re (150 nL, AP: -0.7 mm; ML: 0 mm; DV: -4.3 mm). For chemogenetic inhibition of Re neurons receiving SC projections, AAV1-hSyn-NLS-Cre was bilaterally injected into the SC (200 nL/side, AP: -3.8 mm; ML: ± 0.9 mm; DV: -2.05 mm), and 150 nL of AAV9-hSyn-DIO-hM4Di-EGFP (Braincase, cat#: BC-0626, 5.10E + 12 v.g./mL) was injected into the Re. For chemogenetic activation of Re neurons receiving vLGN/IGL projections, mice were

bilaterally injected with 100 nL/side of AAV1-hSyn-NLS-Cre into the vLGN/IGL and 150 nL of AAV9-EF1 α -DIO-hM3Dq-mCherry (Braincase, cat#: BC-0146, 5.62E + 12 v.g./mL) into the Re. Twenty-one days later, Compound 21 (C21, Tocris Bioscience, 1 mg/kg, dissolved in 0.9% saline) or saline was injected intraperitoneally 1 h before 40 Hz blue light treatment daily. For labeling the Re-projecting vLGN/IGL neurons activated after 1 h acute blue light treatment, we injected 100 nL of AAVretro-hSyn-NLS-Cre (Braincase, cat#: BC-0159, 5E + 12 v.g./mL) into the Re and 150 nL/side of AAV9-hSyn-DIO-EGFP (BrainVTA, cat#: PT-1103, 5E + 12 v.g./mL) into the vLGN/IGL. For in vitro brain slice electrophysiology recording, mice were bilaterally injected with 100 nL/side of AAV1-hSyn-NLS-Cre into the vLGN/IGL and 150 nL of AAV9-hSyn-DIO-EGFP into the Re. For labeling of axonal terminals from vLGN/IGL-targeted Re neurons, we injected 150 nL AAV9-hSyn-DIO-mGFP-T2A-Synaptophysin-mRuby (BrainVTA, cat#: PT-1244, 1.16E + 13 v.g./mL) into the Re, and bilaterally injected 100 nL/side AAV1-hSyn-NLS-Cre into the vLGN/IGL.

Immunofluorescence staining and image analysis

Mice were transcardially perfused with PBS for 2 min and 4% paraformaldehyde in PBS for 5 min at a rate of 10 mL/min. The brains were then harvested and postfixed in 4% paraformaldehyde in PBS overnight at 4 °C, followed by cryoprotection in 30% sucrose in PBS for 2–3 days at 4 °C. 30 μ m coronal brain sections were collected using a cryostat. Two coronal sections containing the dorsal hippocampus (at approximately 1.70 and 1.94 mm posterior to the Bregma) and two sections containing the visual cortex (at approximately 3.16 and 3.40 mm posterior to the Bregma) were sampled for free-floating immunofluorescence staining. The brain regions of interest were determined based on the 4th edition of “the Mouse Brain in Stereotaxic Coordinates” by Paxinos and Franklin⁸⁸. The sections were blocked with a solution containing 5% goat serum, 1% bovine serum albumin, and 0.4% Triton X-100 in PBS for 2 h at room temperature. Subsequently, they were incubated with primary antibodies: c-FOS (Cell Signaling Technology, cat#: 2250, 1:750), A β (clone 6E10, BioLegend, cat#: 803001, 1:2000), GFAP (Abcam, cat#: ab4674, 1:1000), S100 β (Abcam, cat#: ab52642, 1:1000), AQP4 (Millipore, cat#: AB3594, 1:1000), IBA1 (Fujifilm, cat#: 019-19741, 1:1000), CD68 (clone FA-11, Bio-RAD, cat#: MCA1957GA, 1:500) and GFP (Abcam, cat#: ab13970, 1:1000) in the blocking buffer for approximately 24 h at 4 °C. Following this, the tissues were rinsed three times for 10 min each in PBS with 0.4% Triton X-100, and then stained with secondary antibodies in the blocking buffer for 2 h at room temperature. The sections were washed again three times and mounted with glass slides and coverslips.

The dorsal meningeal lymphatic vessels (mLV) attached to the skullcap were harvested and postfixed in 2% PFA at 4 °C overnight. After being peeled off from the skull, the dura mater was blocked in PBS containing 5% normal goat serum, 1% BSA, 0.05% Tween-20, and 0.1% Triton X-100 for 2 h at room temperature. It was then incubated with a primary antibody for LYVE1 (Abcam, cat#: ab14917, 1:500) diluted in PBS containing 1% BSA and 0.5% Triton X-100 at 4 °C overnight. Washes and secondary antibody staining of the meninges were carried out similarly to the staining procedures of brain sections. dCLNs were also harvested, and 30 μ m sections were collected and mounted on glass slides.

Images were acquired using an epi-fluorescent microscope (Eclipse Ni-U, Nikon, Japan), or Zeiss LSM780 confocal microscope (Jena, Germany), and analyzed with ImageJ (version 1.52n, NIH, US). For the assessment of tracer diffusion, the fluorescence intensity and the percentage of area covered by the OVA-Alexa Fluor 647 tracer were analyzed and normalized to total area of brain sections or dCLNs. For the assessment of astrocyte activation, the ratio of GFAP to S100 β fluorescence intensity and the covered area were measured. For the assessment of microglia activation, the

fluorescence intensity, the percentage of covered area, the soma size and the primary process length, as well as CD68 or A β (6E10) colocalization with IBA1-positive microglia, were analyzed. To analyze the primary process length of microglia, 16–20 microglia cells of each brain regions were chosen and the major projection directly coming off from the soma body were measured and averaged. To analyze CD68 within IBA1-labeled microglia, the area of IBA1-labeled microglia was used as ROI to calculate the fluorescence intensity and covered area of CD68 in IBA1. For the assessment of c-FOS and A β (6E10) staining, the analyze particles plugin was used to measure the density of c-FOS-positive cells and the density and the covered area of A β deposits. For the quantification of AQP4 polarization, the lineplot tool was used to analyze 50 μ m segments centered on blood vessels (as identified by vascular-shaped AQP4 localization). Ten vessels of 6 μ m wide (range of 5–8 μ m) were chosen. The baseline fluorescence was defined as the average intensity over 10 μ m, –20 μ m to –10 μ m from peak fluorescence. The polarity was calculated by subtracting baseline fluorescence from the peak intensity of the segment. Average polarity was calculated, and the polarization index of each group were normalized to the WT-Con group⁸⁹. For quantification of the diameter of meningeal lymphatic vessels, 70 individual diameter measurements (40 along the TS + COS and 30 along the SSS) per meninx were calculated by an investigator blinded to the experimental groups, and the averaged value was taken as one data point. For IBA1-labeled microglia co-localized with A β , and c-FOS localized within GFP-labeled neurons, images were manually counted by an investigator blinded to the experimental groups. Pearson correlation analysis of percentage of covered area by OVA in the dCLNs and AQP4 polarization index of each brain regions was performed in R (version 4.4.1), and the bubble chart was generated using ggplot2 (version 3.5.1).

Tissue dissection and metabolite extraction

Female and male 5xFAD mice aged 4 months, along with their wild-type littermates, were used. Mice were transcardially perfused with ice-cold PBS for 1 min under anesthesia. Their brains were then quickly dissected, and the hippocampi were harvested in an ice-cold dissection buffer for subsequent metabolite extraction and LC-MS analysis, which were carried out by BIOTREE (Shanghai, China). 30 mg of each sample was added sequentially with 200 μ L water and 480 μ L extract solution (composed of a 5:1 volume ratio of methyl-tert-butyl ether to methanol). After vortex mixing for 30 s, the samples were sonicated in an ice-water bath for 10 min. This homogenization and sonication process was repeated 3 times, after which the samples were incubated at –40 °C for 1 h and then centrifuged at 845 \times g for 15 min at 4 °C. 300 μ L of supernatant was transferred to a new tube and dried in a vacuum concentrator at 37 °C. The dried samples were then reconstituted in 100 μ L solution of dichloromethane/methanol mixture (1:1 volume ratio) through vortex mixing for 30 s and sonication for 10 min in an ice-water bath, prior to centrifugation at 15,871 \times g for 15 min at 4 °C. 75 μ L of supernatant was transferred to a fresh glass vial for LC/MS analysis. A quality control sample was prepared by combining equal volumes (20 μ L) of supernatants from all the samples.

LC-MS/MS lipidomic analysis

LC-MS/MS analyses were conducted utilizing an UHPLC system (model 1290, Agilent Technologies), equipped with a Kinetex C18 column (2.1 \times 100 mm, 1.7 μ m, Phenomen). Two mobile phases were employed: A, composed of 40% water, 60% acetonitrile, and 10 mmol/L ammonium formate, and B, consisting of 10% acetonitrile and 90% isopropanol, with 50 mL of 10 mmol/L ammonium formate added per 1000 mL of mixed solvent. Elution was carried out under the following gradient conditions: 0–1.0 min, 40% B; 1.0–12.0 min, 40–100% B; 12.0–13.5 min, 100% B; 13.5–13.7 min, 100–40% B;

13.7–18.0 min, 40% B. The column was maintained at 55 °C, with an auto-sampler temperature of 4 °C. The injection volume was 2 µL for both positive and negative modes. Raw data were converted to mzXML format using the ‘msconvert’ program (ProteoWizard). Peak detection, extraction, alignment, and integration were executed using the CentWave algorithm in XCMS, with a minfrac annotation setting of 0.5, and cutoff of 0.3. Lipid identification was conducted through spectral matching using the LipidBlast library, developed in R and based on XCMS (version 3.2). Partial least squares discrimination analysis (PLS-DA) was applied (ropls, version 1.34.0) to reveal lipid profile variation among the three groups. For paired comparison, Orthogonal Partial Least Squares-Discriminant Analysis (OPLS-DA) was performed on the positive- and negative-mode MS data that had been centered and scaled to unit variance scaling. Differentially expressed lipids were identified based on the variable importance in projection (VIP) scores from pairwise OPLS-DA analysis (SIMCA, version 18.0.1, Sartorius Stedim Data Analytics AB, Umea, Sweden) and Student’s *t*-test comparisons, with a cutoff of $p < 0.05$ and $VIP > 1$. The data were visualized using the ggplot2 package (version 3.5.0), pheatmap package (version 1.0.12) and the ggpie package (version 0.2.5) in R (version 4.3.3). The pie chart represents the proportion of differentially expressed lipids belonging to each category relative to the total number of differentially expressed lipids. Bar plots were also employed to present the sum of relative percent difference of either increased or decreased lipid species in the content of each lipid category between groups. Relative difference (%) = (fold change - 1) × 100.

In vitro electrophysiology

280 µm coronal slices containing the Re were obtained through sectioning in an ice-cold buffer (in mM: 250 sucrose, 2 KCl, 1.3 NaH₂PO₄, 10 D-glucose, 26 NaHCO₃, 0.2 CaCl₂, 12 MgSO₄, and 290–300 mOsm; pH = 7.4) with a Leica VT1200S vibratome. The brain slices were incubated in artificial cerebrospinal fluid (aCSF, in mM: 126 NaCl, 3 KCl, 1.26 NaH₂PO₄, 10 D-glucose, 26 NaHCO₃, 2 CaCl₂, 1 MgSO₄, and 290–300 mOsm, at pH 7.4) for 0.5 h at 34 °C, followed by 1 h incubation at room temperature in aCSF, bubbled with 95% O₂, 5% CO₂.

The slices were then transferred to the recording chamber and continuously perfused with aCSF at room temperature during recording. The patch pipettes (resistance: 3–7 MΩ) were filled with intracellular solution (in mM: 130 K-gluconate, 20 KCl, 10 HEPES, 0.2 EGTA, 4 MgATP, 0.3 NaGTP, 10 Na₂-phosphocreatine; pH = 7.4). Whole-cell patch clamp recordings were carried out using a Multi-Clamp 700B amplifier under the infrared-differential interference contrast microscope (ECLIPSE FN1, Nikon). Signals were filtered at 3 kHz and sampled at 10 kHz with a Digidata1550B. Data acquisition and analyses were performed using the software pClamp 10.2 (Molecular Devices).

All recordings were carried out in current-clamp mode. To measure the input–output relationship, an 800 ms long stepwise increasing current, starting at –20 pA and increasing by 10 pA in 23 steps up to +200 pA was injected and the resulting firing frequency was noted. To measure the input resistance, a short-duration (50 ms), stepwise (increasing by 5 pA each time) current was injected into the cell to elicit an action potential. Rheobase current was quantified as the minimal depolarizing current sufficient to elicit a single action potential. To record the spontaneous activity, the frequency of firing was determined over 70 s without current injection.

ELISA

Mice were transcardially perfused with ice-cold PBS for 2 min. Hippocampus tissues were quickly harvested and homogenized in tissue homogenization buffer (2 mM Tris, 250 mM sucrose, 0.5 mM EDTA, 0.5 mM EGTA in RNase-free H₂O) containing protease and

phosphatase inhibitor cocktail (Thermo Scientific, cat#: 78443). The homogenates were mixed with 0.4% diethylamine (Macklin, cat#:D807382) at 1:1 (vol/vol) ratio, and ultracentrifuged at 135,000 × *g* for 1 h at 4 °C. The supernatants were transferred and neutralized with 0.5 M Tris-HCl (pH 6.8) at 10:1 (vol/vol) supernatant to Tris-HCl ratio. Concentration of soluble Aβ₄₂ was assessed using an enzyme-linked immunosorbent assay kit (Elabsience, cat#: E-EL-H0543c), followed by normalization to protein concentration determined by a BCA protein assay kit (Beyotime, cat#: P0009).

Statistical analyses

Statistical analysis was performed in Prism v8.0 (GraphPad Software, Boston, MA). The Shapiro–Wilk test or the Kolmogorov–Smirnov test was used to evaluate the normality of the datasets. The ROUT ($Q = 5\%$) method was applied to identify and exclude outliers in the datasets. For two-group comparisons, two-tailed unpaired Student’s *t* test was used for normally distributed datasets, and Mann–Whitney test was used for non-normally distributed datasets. For multiple-group comparisons, one-way ANOVA with Tukey’s or Fisher’s LSD *post hoc* test was used for normally distributed datasets, and Kruskal–Wallis test with Dunn’s *post hoc* test was used for non-normally distributed datasets. For the analysis of electrophysiology data, two-way ANOVA followed by Bonferroni’s *post hoc* test was used to compare the current evoked-action potentials and Fisher’s exact test was used to compare the percentage of silent and spontaneous cells. For the analysis of MRI data, two-way ANOVA with Tukey’s *post hoc* test was used to compare main column effect. $P < 0.05$ was considered as statistically significant.

Reporting summary

Further information on research design is available in the Nature Portfolio Reporting Summary linked to this article.

Data availability

All data generated in this study are provided in the Source Data. The LC-MS/MS lipidomics data generated in this study have been deposited in the Open Archive for Miscellaneous Data (OMIX) repository under accession code [OMIX008180](https://doi.org/10.1002/omix.0008180). Source data are provided with this paper.

References

- 2023 Alzheimer’s disease facts and figures. *Alzheimers Dement* **19**, 1598–1695 <https://doi.org/10.1002/alz.13016> (2023).
- Ren, R. et al. The China Alzheimer Report 2022. *Gen. Psychiatr.* **35**, e100751 (2022).
- van Dyck, C. H. et al. Lecanemab in early Alzheimer’s disease. *N. Engl. J. Med.* **388**, 9–21 (2023).
- Swanson, C. J. et al. A randomized, double-blind, phase 2b proof-of-concept clinical trial in early Alzheimer’s disease with lecanemab, an anti-Aβeta protofibril antibody. *Alzheimers Res. Ther.* **13**, 80 (2021).
- Forbes, D. et al. Light therapy for managing cognitive, sleep, functional, behavioural, or psychiatric disturbances in dementia. *Cochrane Database Syst. Rev.* CD003946 <https://doi.org/10.1002/14651858.CD003946.pub3> (2009).
- Forbes, D., Blake, C. M., Thiessen, E. J., Peacock, S. & Hawranik, P. Light therapy for improving cognition, activities of daily living, sleep, challenging behaviour, and psychiatric disturbances in dementia. *Cochrane Database Syst. Rev.* **2014**, CD003946 (2014).
- Zang, L. et al. The effect of light therapy on sleep disorders and psychobehavioral symptoms in patients with Alzheimer’s disease: a meta-analysis. *PLoS One* **18**, e0293977 (2023).
- Blanco-Duque, C., Chan, D., Kahn, M. C., Murdock, M. H. & Tsai, L. H. Audiovisual gamma stimulation for the treatment of neurodegeneration. *J. Intern Med.* **295**, 146–170 (2024).

9. Berson, D. M., Dunn, F. A. & Takao, M. Phototransduction by retinal ganglion cells that set the circadian clock. *Science* **295**, 1070–1073 (2002).
10. Vandewalle, G., Maquet, P. & Dijk, D. J. Light as a modulator of cognitive brain function. *Trends Cogn. Sci.* **13**, 429–438 (2009).
11. Viola, A. U., James, L. M., Schlangen, L. J. & Dijk, D. J. Blue-enriched white light in the workplace improves self-reported alertness, performance and sleep quality. *Scand. J. Work Environ. Health* **34**, 297–306 (2008).
12. Kim, S. J. et al. Positive effect of timed blue-enriched white light on sleep and cognition in patients with mild and moderate Alzheimer's disease. *Sci. Rep.* **11**, 10174 (2021).
13. Chan, D. et al. Gamma frequency sensory stimulation in mild probable Alzheimer's dementia patients: results of feasibility and pilot studies. *PLoS One* **17**, e0278412 (2022).
14. Adaikkan, C. et al. Gamma entrainment binds higher-order brain regions and offers neuroprotection. *Neuron* **102**, 929–943.e928 (2019).
15. Iaccarino, H. F. et al. Gamma frequency entrainment attenuates amyloid load and modifies microglia. *Nature* **540**, 230–235 (2016).
16. Soula, M. et al. Forty-hertz light stimulation does not entrain native gamma oscillations in Alzheimer's disease model mice. *Nat. Neurosci.* **26**, 570–578 (2023).
17. Iff, J. J. et al. A paravascular pathway facilitates CSF flow through the brain parenchyma and the clearance of interstitial solutes, including amyloid beta. *Sci. Transl. Med.* **4**, 147ra111 (2012).
18. Rasmussen, M. K., Mestre, H. & Nedergaard, M. Fluid transport in the brain. *Physiol. Rev.* **102**, 1025–1151 (2022).
19. Hablitz, L. M. & Nedergaard, M. The glymphatic system. *Curr. Biol.* **31**, R1371–R1375 (2021).
20. Mestre, H. et al. Aquaporin-4-dependent glymphatic solute transport in the rodent brain. *Elife* **7** <https://doi.org/10.7554/eLife.40070> (2018).
21. Peng, W. et al. Suppression of glymphatic fluid transport in a mouse model of Alzheimer's disease. *Neurobiol. Dis.* **93**, 215–225 (2016).
22. Xu, P. et al. Extracellular ATP enhances radiation-induced brain injury through microglial activation and paracrine signaling via P2X7 receptor. *Brain Behav. Immun.* **50**, 87–100 (2015).
23. de Leon, M. J. et al. Cerebrospinal fluid clearance in Alzheimer disease measured with dynamic PET. *J. Nucl. Med.* **58**, 1471–1476 (2017).
24. Zeppenfeld, D. M. et al. Association of perivascular localization of aquaporin-4 with cognition and Alzheimer disease in aging brains. *JAMA Neurol.* **74**, 91–99 (2017).
25. van Veluw, S. J. et al. Vasomotion as a driving force for paravascular clearance in the awake mouse brain. *Neuron* **105**, 549–561.e545 (2020).
26. Williams, S. D. et al. Neural activity induced by sensory stimulation can drive large-scale cerebrospinal fluid flow during wakefulness in humans. *PLoS Biol.* **21**, e3002035 (2023).
27. Oakley, H. et al. Intraneuronal beta-amyloid aggregates, neurodegeneration, and neuron loss in transgenic mice with five familial Alzheimer's disease mutations: potential factors in amyloid plaque formation. *J. Neurosci.* **26**, 10129–10140 (2006).
28. Wang, G. et al. Short-term acute bright light exposure induces a prolonged anxiogenic effect in mice via a retinal ipRGC-CeA circuit. *Sci. Adv.* **9**, eadf4651 (2023).
29. Eichenbaum, H. On the integration of space, time, and memory. *Neuron* **95**, 1007–1018 (2017).
30. Griffin, A. L. The nucleus reuniens orchestrates prefrontal-hippocampal synchrony during spatial working memory. *Neurosci. Biobehav. Rev.* **128**, 415–420 (2021).
31. Todd, T. P., Fournier, D. I. & Bucci, D. J. Retrosplenial cortex and its role in cue-specific learning and memory. *Neurosci. Biobehav. Rev.* **107**, 713–728 (2019).
32. Basso, M. A., Bickford, M. E. & Cang, J. Unraveling circuits of visual perception and cognition through the superior colliculus. *Neuron* **109**, 918–937 (2021).
33. Resulaj, A. Projections of the mouse primary visual cortex. *Front. Neural Circuits* **15**, 751331 (2021).
34. Hu, H., Cui, Y. & Yang, Y. Circuits and functions of the lateral habenula in health and in disease. *Nat. Rev. Neurosci.* **21**, 277–295 (2020).
35. Antila, S. et al. Development and plasticity of meningeal lymphatic vessels. *J. Exp. Med.* **214**, 3645–3667 (2017).
36. Zhu, B. et al. MMP-9 inhibition alleviates postoperative cognitive dysfunction by improving glymphatic function via regulating AQP4 polarity. *Int Immunopharmacol.* **126**, 111215 (2024).
37. Gomolka, R. S. et al. Loss of aquaporin-4 results in glymphatic system dysfunction via brain-wide interstitial fluid stagnation. *Elife* **12** <https://doi.org/10.7554/eLife.82232> (2023).
38. Simon, M. et al. Loss of perivascular aquaporin-4 localization impairs glymphatic exchange and promotes amyloid beta plaque formation in mice. *Alzheimers Res. Ther.* **14**, 59 (2022).
39. Sofroniew, M. V. & Vinters, H. V. Astrocytes: biology and pathology. *Acta Neuropathol.* **119**, 7–35 (2010).
40. Blaszczyk, L. et al. Sequential alteration of microglia and astrocytes in the rat thalamus following spinal nerve ligation. *J. Neuroinflamm.* **15**, 349 (2018).
41. Huang, X. et al. A visual circuit related to the nucleus reuniens for the spatial-memory-promoting effects of light treatment. *Neuron* **109**, 347–362.e347 (2021).
42. Salay, L. D. & Huberman, A. D. Divergent outputs of the ventral lateral geniculate nucleus mediate visually evoked defensive behaviors. *Cell Rep.* **37**, 109792 (2021).
43. Zhang, S. et al. Organization of long-range inputs and outputs of frontal cortex for top-down control. *Nat. Neurosci.* **19**, 1733–1742 (2016).
44. Rangroo Thrane, V. et al. Paravascular microcirculation facilitates rapid lipid transport and astrocyte signaling in the brain. *Sci. Rep.* **3**, 2582 (2013).
45. Akyol, S. et al. Lipid profiling of Alzheimer's disease brain highlights enrichment in Glycerol(phospho)lipid, and sphingolipid metabolism. *Cells* **10**, <https://doi.org/10.3390/cells10102591> (2021).
46. Batra, R. et al. The landscape of metabolic brain alterations in Alzheimer's disease. *Alzheimers Dement* **19**, 980–998 (2023).
47. Michno, W. et al. Spatial neuropilidomics at the single amyloid-beta plaque level in postmortem human Alzheimer's disease brain. *ACS Chem. Neurosci.* **15**, 877–888 (2024).
48. Haney, M. S. et al. APOE4/4 is linked to damaging lipid droplets in Alzheimer's disease microglia. *Nature* **628**, 154–161 (2024).
49. Forstl, H. & Kurz, A. Clinical features of Alzheimer's disease. *Eur. Arch. Psychiatry Clin. Neurosci.* **249**, 288–290 (1999).
50. Srivastava, S., Ahmad, R. & Khare, S. K. Alzheimer's disease and its treatment by different approaches: a review. *Eur. J. Med Chem.* **216**, 113320 (2021).
51. Riemersma-van der Lek, R. F. et al. Effect of bright light and melatonin on cognitive and noncognitive function in elderly residents of group care facilities: a randomized controlled trial. *JAMA* **299**, 2642–2655 (2008).
52. Paus, S. et al. Bright light therapy in Parkinson's disease: a pilot study. *Mov. Disord.* **22**, 1495–1498 (2007).
53. Lam, R. W. et al. Efficacy of bright light treatment, fluoxetine, and the combination in patients with nonseasonal major depressive disorder: a randomized clinical trial. *JAMA Psychiatry* **73**, 56–63 (2016).
54. Yamadera, H. et al. Effects of bright light on cognitive and sleep-wake (circadian) rhythm disturbances in Alzheimer-type dementia. *Psychiatry Clin. Neurosci.* **54**, 352–353 (2000).

55. Graf, A. et al. The effects of light therapy on mini-mental state examination scores in demented patients. *Biol. Psychiatry* **50**, 725–727 (2001).
56. Burns, A., Allen, H., Tomenson, B., Duignan, D. & Byrne, J. Bright light therapy for agitation in dementia: a randomized controlled trial. *Int. Psychogeriatr.* **21**, 711–721 (2009).
57. Hatori, M. & Panda, S. The emerging roles of melanopsin in behavioral adaptation to light. *Trends Mol. Med.* **16**, 435–446 (2010).
58. Huang, L. et al. A visual circuit related to habenula underlies the antidepressive effects of light therapy. *Neuron* **102**, 128–142.e128 (2019).
59. Sun, X. et al. 40 Hz light flickering facilitates the glymphatic flow via adenosine signaling in mice. *Cell Discov.* **10**, 81 (2024).
60. Park, S. S. et al. Physical exercise during exposure to 40-Hz light flicker improves cognitive functions in the 3xTg mouse model of Alzheimer's disease. *Alzheimers Res. Ther.* **12**, 62 (2020).
61. Lin, Z. et al. 40-Hz blue light changes hippocampal activation and functional connectivity underlying recognition memory. *Front Hum. Neurosci.* **15**, 739333 (2021).
62. Ishida, K. et al. Glymphatic system clears extracellular tau and protects from tau aggregation and neurodegeneration. *J. Exp. Med.* **219** <https://doi.org/10.1084/jem.20211275> (2022).
63. Lee, A. et al. Aβ₄₂ oligomers trigger synaptic loss through CAMKK2-AMPK-dependent effectors coordinating mitochondrial fission and mitophagy. *Nat. Commun.* **13**, 4444 (2022).
64. Da Mesquita, S. et al. Functional aspects of meningeal lymphatics in ageing and Alzheimer's disease. *Nature* **560**, 185–191 (2018).
65. Wang, L. et al. Deep cervical lymph node ligation aggravates AD-like pathology of APP/PS1 mice. *Brain Pathol.* **29**, 176–192 (2019).
66. Chen, G. F. et al. Amyloid beta: structure, biology and structure-based therapeutic development. *Acta Pharm. Sin.* **38**, 1205–1235 (2017).
67. Villemagne, V. L. et al. Amyloid beta deposition, neurodegeneration, and cognitive decline in sporadic Alzheimer's disease: a prospective cohort study. *Lancet Neurol.* **12**, 357–367 (2013).
68. Jacquemyn, J., Ralhan, I. & Ioannou, M. S. Driving factors of neuronal ferroptosis. *Trends Cell Biol.* **34**, 535–546 (2024).
69. Pope, L. E. & Dixon, S. J. Regulation of ferroptosis by lipid metabolism. *Trends Cell Biol.* **33**, 1077–1087 (2023).
70. Qi, G. et al. ApoE4 impairs neuron-astrocyte coupling of fatty acid metabolism. *Cell Rep.* **34**, 108572 (2021).
71. Ioannou, M. S. et al. Neuron-astrocyte metabolic coupling protects against activity-induced fatty acid toxicity. *Cell* **177**, 1522–1535.e1514 (2019).
72. Si, X. et al. Matrix metalloproteinase-9 inhibition prevents aquaporin-4 depolarization-mediated glymphatic dysfunction in Parkinson's disease. *J. Adv. Res.* **56**, 125–136 (2024).
73. Hussain, R. et al. Potentiating glymphatic drainage minimizes post-traumatic cerebral oedema. *Nature* **623**, 992–1000 (2023).
74. Harrison, I. F. et al. Impaired glymphatic function and clearance of tau in an Alzheimer's disease model. *Brain* **143**, 2576–2593 (2020).
75. Nedergaard, M. & Goldman, S. A. Glymphatic failure as a final common pathway to dementia. *Science* **370**, 50–56 (2020).
76. Buccellato, F. R., D'Anca, M., Serpente, M., Arighi, A. & Galimberti, D. The role of glymphatic system in Alzheimer's and Parkinson's disease pathogenesis. *Biomedicines* **10** <https://doi.org/10.3390/biomedicines10092261> (2022).
77. Peters, M. E. & Lyketsos, C. G. The glymphatic system's role in traumatic brain injury-related neurodegeneration. *Mol. Psychiatry* **28**, 2707–2715 (2023).
78. Martorell, A. J. et al. Multi-sensory gamma stimulation ameliorates Alzheimer's-associated pathology and improves cognition. *Cell* **177**, 256–271.e222 (2019).
79. Steinberg, M. et al. Point and 5-year period prevalence of neuropsychiatric symptoms in dementia: the Cache County Study. *Int. J. Geriatr. Psychiatry* **23**, 170–177 (2008).
80. Lyketsos, C. G. et al. Neuropsychiatric symptoms in Alzheimer's disease. *Alzheimers Dement* **7**, 532–539 (2011).
81. Orsel, K. et al. Psychotropic drugs use and psychotropic polypharmacy among persons with Alzheimer's disease. *Eur. Neuropsychopharmacol.* **28**, 1260–1269 (2018).
82. Majid, O. et al. Population pharmacokinetics and exposure-response analyses of safety (ARIA-E and isolated ARIA-H) of lecanemab in subjects with early Alzheimer's disease. *CPT Pharmacometrics Syst. Pharmacol.* <https://doi.org/10.1002/psp4.13224> (2024).
83. Burke, J. F., Kerber, K. A., Langa, K. M., Albin, R. L. & Kotagal, V. Lecanemab: looking before we leap. *Neurology* **101**, 661–665 (2023).
84. Murdock, M. H. et al. Multisensory gamma stimulation promotes glymphatic clearance of amyloid. *Nature* **627**, 149–156 (2024).
85. Woo, J. et al. Astrocytic water channel aquaporin-4 modulates brain plasticity in both mice and humans: a potential gliogenetic mechanism underlying language-associated learning. *Mol. Psychiatry* **23**, 1021–1030 (2018).
86. Da Mesquita, S. et al. Meningeal lymphatics affect microglia responses and anti-Aβ immunotherapy. *Nature* **593**, 255–260 (2021).
87. Gardner, D. J., Davis, J. A., Weina, P. J. & Theune, B. Comparison of tribromoethanol, ketamine/acetylpromazine, Telazol/xylazine, pentobarbital, and methoxyflurane anesthesia in HSD:ICR mice. *Lab Anim. Sci.* **45**, 199–204 (1995).
88. George Paxinos, K. B. J. F. *The Mouse Brain in Stereotaxic Coordinates* (Academic Press, 2001).
89. Hablitz, L. M. et al. Circadian control of brain glymphatic and lymphatic fluid flow. *Nat. Commun.* **11**, 4411 (2020).

Acknowledgements

We thank the animal facility and the core facility of the Zhongshan School of Medicine, Sun Yat-sen University. We thank Dr. Yanqiu Feng at School of Biomedical Engineering in Southern Medical University for technical support of MRI experiments. We thank Dr. Ni Fan at the Affiliated Brain Hospital of Guangzhou Medical University for technical support of light therapy. We thank all members of the Lin lab, Ye lab, Wu lab and Ma lab for discussion and technical assistance during the execution of this project. This work was supported by the National Natural Science Foundation of China (81972967 to W.J.L., 32271068 to X.Y., and 82172526 to W.W., 82272586 to Y.L.), Science and Technology Program of Guangzhou (202007030001 to B.L., X.Y., and W.J.L.), the Science and Technology Planning Project of Guangdong (2023B1212060013 and 2020B1212030004 to W.J.L.), Guangdong Natural Science Foundation (2024A1515011474 to X.Y.), the Science and Technology Planning Project of Guangdong Province (2023B1212060018 to B.L., X.Y., and W.J.L.), and Guangdong Project (2019QN01Y202 to X.Y.).

Author contributions

W.J.L., X.Y., W.W. and J.M. conceptualized and designed the research project; W.W., Y.Z., X.C., X.X., Y.Z., Q.T., Y.Y., and C.X. performed the experiments; Y.Z., X.C., X.X., Y.Z., Y.Y., J.P., J.J., Z.Z., H.H., Y.L., and B.L. contributed to the analysis and interpretation of data; Y.Z., W.J.L. and X.Y. wrote the manuscript with input and approval from all the authors.

Competing interests

The authors declare no competing interests.

Additional information

Supplementary information The online version contains supplementary material available at <https://doi.org/10.1038/s41467-024-55678-w>.

Correspondence and requests for materials should be addressed to Wen Wu, Junxian Ma, Xiaojing Ye or Wei-Jye Lin.

Peer review information *Nature Communications* thanks Chaoran Ren and the other, anonymous, reviewers for their contribution to the peer review of this work. A peer review file is available.

Reprints and permissions information is available at <http://www.nature.com/reprints>

Publisher's note Springer Nature remains neutral with regard to jurisdictional claims in published maps and institutional affiliations.

Open Access This article is licensed under a Creative Commons Attribution-NonCommercial-NoDerivatives 4.0 International License, which permits any non-commercial use, sharing, distribution and reproduction in any medium or format, as long as you give appropriate credit to the original author(s) and the source, provide a link to the Creative Commons licence, and indicate if you modified the licensed material. You do not have permission under this licence to share adapted material derived from this article or parts of it. The images or other third party material in this article are included in the article's Creative Commons licence, unless indicated otherwise in a credit line to the material. If material is not included in the article's Creative Commons licence and your intended use is not permitted by statutory regulation or exceeds the permitted use, you will need to obtain permission directly from the copyright holder. To view a copy of this licence, visit <http://creativecommons.org/licenses/by-nc-nd/4.0/>.

© The Author(s) 2024

¹Department of Rehabilitation Medicine, Zhujiang Hospital, Southern Medical University, Guangzhou, China. ²Department of Clinical and Rehabilitation Medicine, Guiyang Healthcare Vocational University, Guizhou, China. ³Faculty of Forensic Medicine, Zhongshan School of Medicine, Sun Yat-sen University, Guangzhou, China. ⁴Guangdong Province Translational Forensic Medicine Engineering Technology Research Center, Sun Yat-sen University, Guangzhou, China. ⁵Guangdong Provincial Key Laboratory of Brain Function and Disease, Zhongshan School of Medicine, Sun Yat-sen University, Guangzhou, China. ⁶Brain Research Center, Sun Yat-sen Memorial Hospital, Sun Yat-sen University, Guangzhou, China. ⁷Guangdong Provincial Key Laboratory of Malignant Tumor Epigenetics and Gene Regulation, Guangdong-Hong Kong Joint Laboratory for RNA Medicine, Medical Research Center, Sun Yat-sen Memorial Hospital, Sun Yat-sen University, Guangzhou, China. ⁸Nanhai Translational Innovation Center of Precision Immunology, Sun Yat-sen Memorial Hospital, Foshan, China. ⁹Guangdong Mental Health Center, Guangdong Provincial People's Hospital (Guangdong Academy of Medical Sciences), Southern Medical University, Guangzhou, China. ¹⁰Department of Rehabilitation Medicine, the Sixth Affiliated Hospital, Sun Yat-sen University, Guangzhou, China. ¹¹Guangdong Provincial Clinical Research Center for Rehabilitation Medicine, Guangzhou, China. ¹²Biomedical Innovation Center, the Sixth Affiliated Hospital, Sun Yat-sen University, Guangzhou, China. ¹³Advanced Medical Technology Center, the First Affiliated Hospital, Zhongshan School of Medicine, Sun Yat-Sen University, Guangzhou, China. ¹⁴Key Laboratory of Human Microbiome and Chronic Diseases (Sun Yat-Sen University), Ministry of Education, Guangzhou, China. ¹⁵Tianfu Xinglong Lake Laboratory, Chengdu, China. ¹⁶These authors contributed equally: Wen Wu, Yubai Zhao, Xin Cheng. ✉ e-mail: wuwen66@163.com; 931616518@qq.com; yexiaoj8@mail.sysu.edu.cn; linwj26@mail.sysu.edu.cn